

Decreasing Trend and Hemispheric Symmetry of Earth's Albedo

- A Brief Review -

HAYASAKA, Tadahiro
Graduate School of Science/Tohoku University
EORC/JAXA

Kobe University CPS Seminar, 4 July 2023

Questions

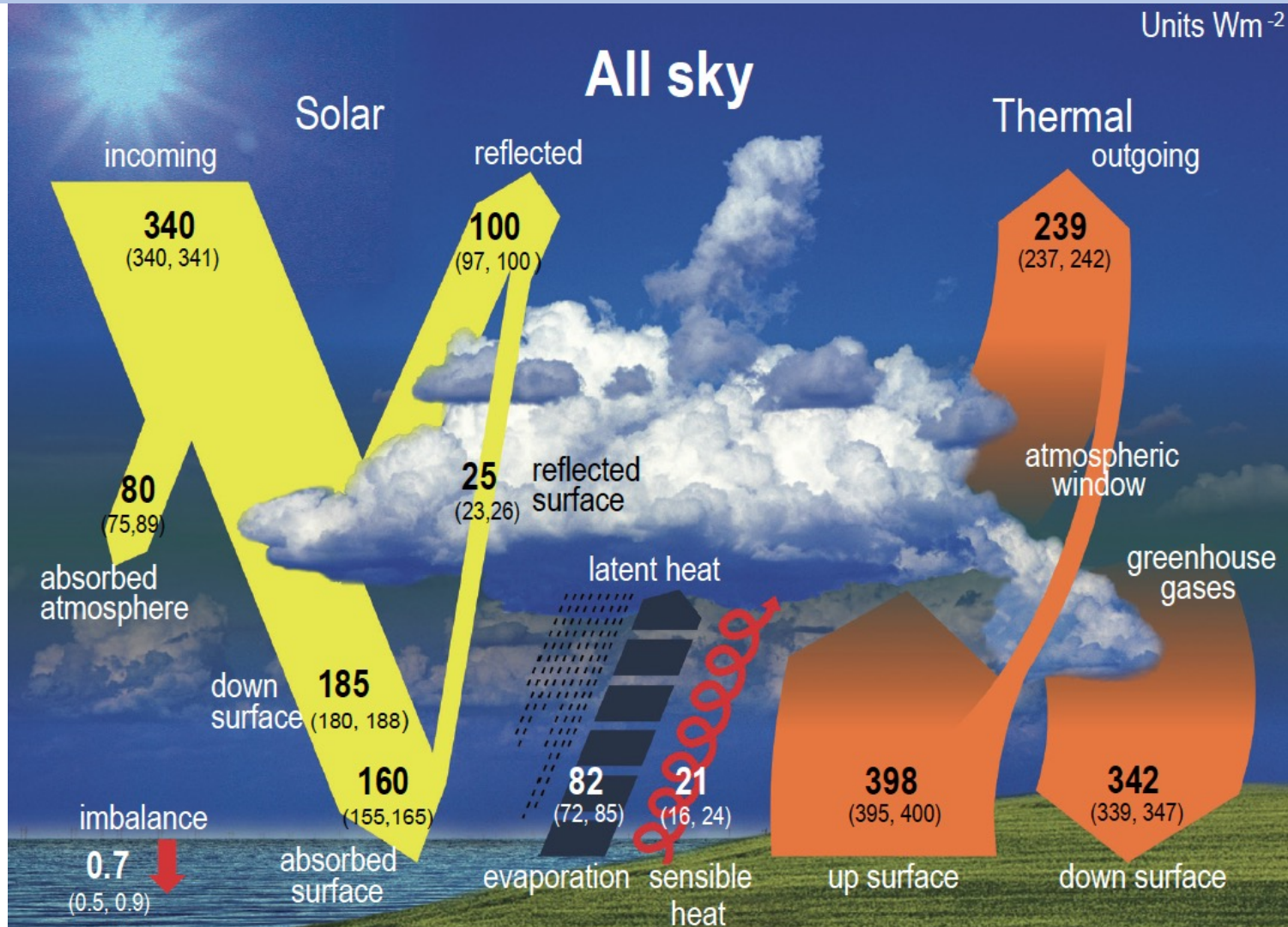
- Is it true that the Earth's albedo is decreasing?
- What are the details of the spatio-temporal variation of the Earth's albedo?
- Does hemispheric symmetry of the Earth's albedo hold?
- Is the decrease in Earth's albedo consistent with climate system?
- What are the factors contributing to the decrease in the Earth's albedo?

Contents

- Importance of the Earth's albedo study
- History of the Earth's albedo study
- Recent satellite observations of the Earth's albedo
- Clouds and the Earth's Radiant Energy System (CERES)
- Variations in the Earth's albedo in the 21st century
- Symmetry of albedo between Northern Hemisphere and Southern Hemisphere
- Discussion

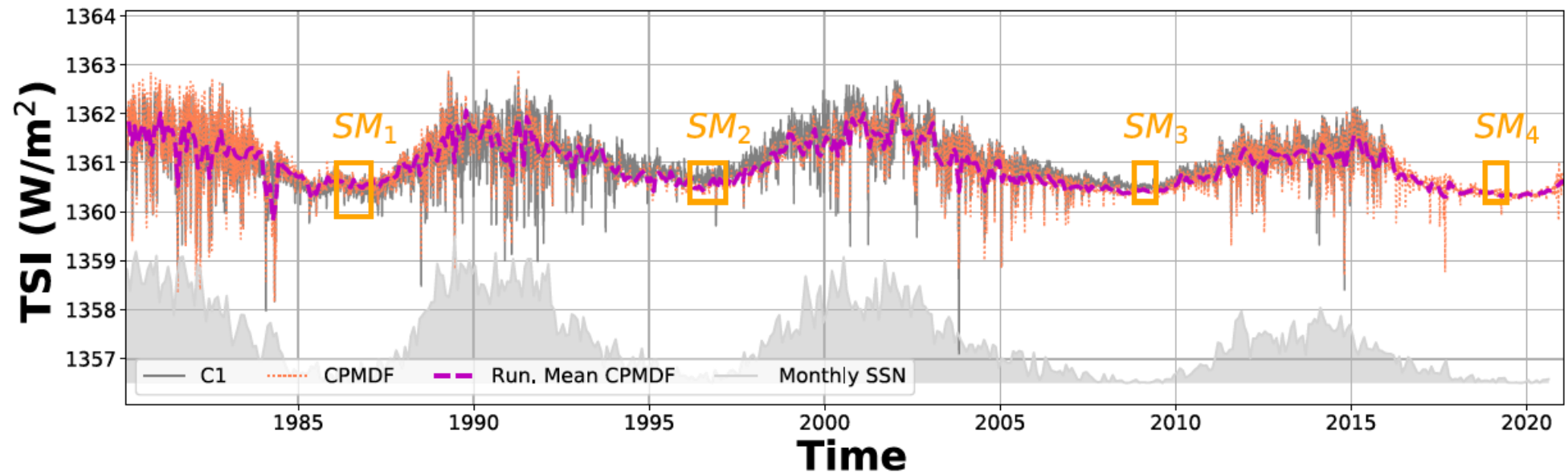
Global Energy Flows (Wm^{-2})

Albedo = 29.4%



(IPCC-AR6, 2021)

Total Solar Irradiance Change for 1980-2020



Amplitude of total solar irradiance is quite small $\sim 0.1\%$

Trend is $\sim -0.004 \pm 0.004 \text{ W}/(\text{m}^2\text{yr})$

SM: Solar minima for each solar cycle

History of Earth's Albedo Study

Table 1. Summary of Milestone Studies of the Earth's Albedo That Highlight the Steps in the Evolution Toward Today's Estimate

Investigation	Albedo	Comments
<i>Abbot and Fowle</i> [1908]	0.37	Forced to make gross assumptions about cloudiness
<i>Dines</i> [1917]	0.50	Influenced by balloon measurements
<i>Aldrich</i> [1922]	0.43	Cloud albedo of 0.78 inferred from measurements of fog below Mount Wilson
<i>Simpson</i> [1929]	0.43	Adopted from Aldrich, recognized importance of water vapor and variations with latitude
<i>Fritz</i> [1950] and <i>Robinson</i> [1958]	0.35	Refined variation with latitude
<i>Houghton</i> [1954]	0.34	Minimum value of 0.28 in subtropics, 0.67 polar
<i>London</i> [1957]	0.32	Offered a refined zonal structure
<i>Very</i> [1912] and <i>Danjon</i> [1928, 1936]	0.89; 0.39, 0.29	Extrapolated earthshine measurements
<i>Vonder Haar and Suomi</i> [1971]	0.30	First estimate from research satellite measurements
ERBE, CERES, 1984–up to present	0.29	From dedicated Earth radiation budget observing systems

Table 2. Annually Averaged Reflected Fluxes Over the Regions Indicated^a

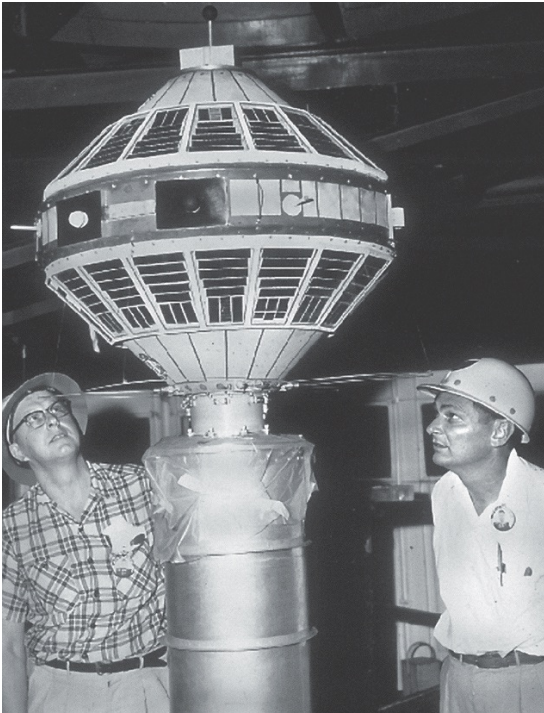
Averaging Scale	Total		Atmosphere		Surface	
	Flux	$\sigma(x)$	Flux	$\sigma(x)$	Flux	$\sigma(x)$
Global	99.7	0.23	86.9	0.29	12.9	0.10
Tropics (30°N–30°S)	94.3	0.32	82.27	0.37	12.1	0.09
Midlatitude NH(30°–60°N)	103.8	0.52	91.5	0.53	12.3	0.15
Midlatitude SH(30°–60°S)	104.1	0.56	98.9	0.65	5.26	0.10
Polar NH (60°–90°N)	97.0	0.87	78.7	0.87	19.1	0.47
Polar SH (60°–90°N)	118.8	0.68	84.4	1.26	35.5	0.97

^aThe TOA reflected flux ($W m^{-2}$) and the contributions to this flux by scattering from the atmosphere and reflection from the surface are given. The standard deviation of the deseasonalized flux as defined by (9) is also given.

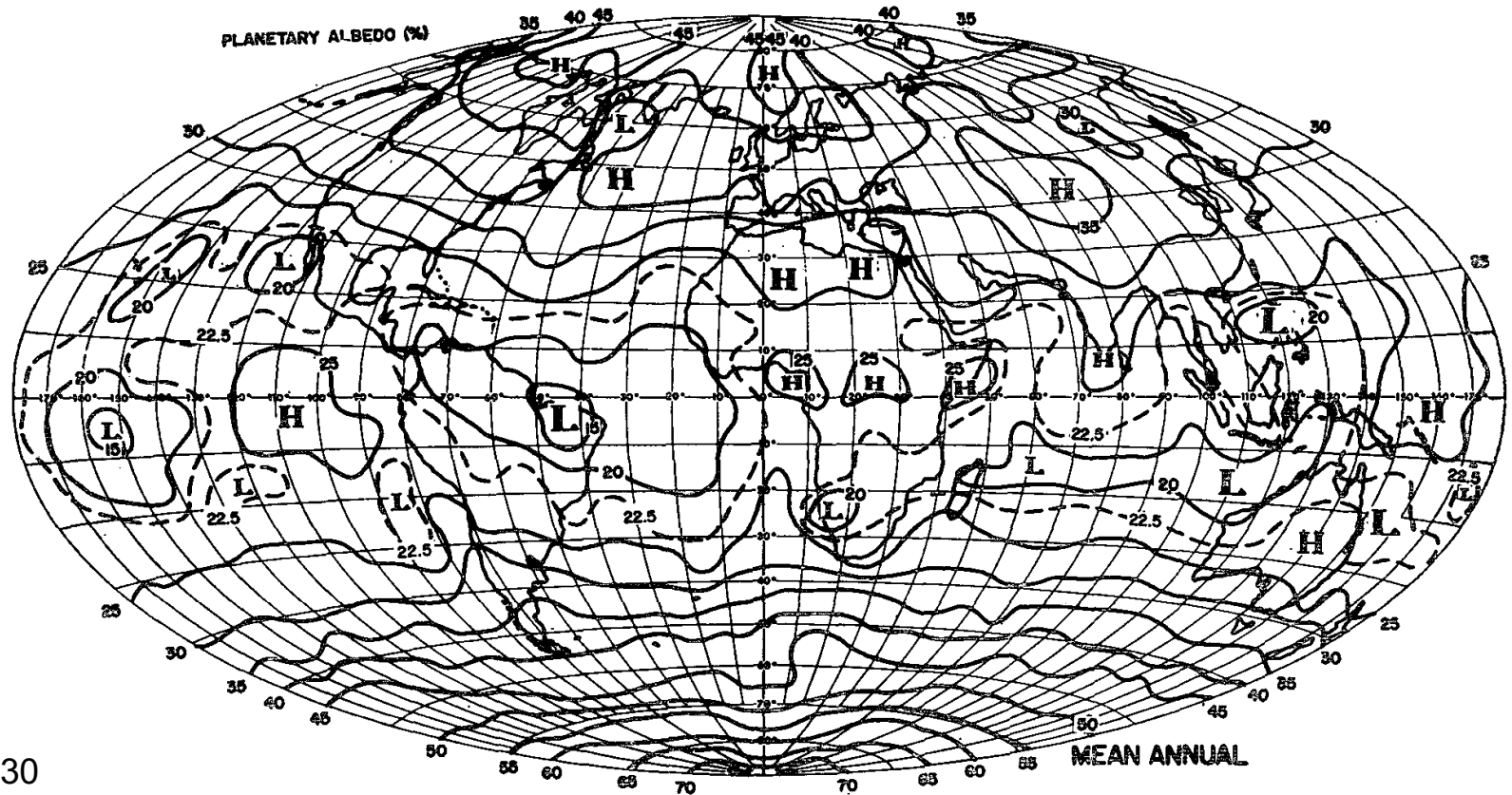
The Northern and Southern Hemispheres (NH, SH) reflect the same amount of sunlight within $\sim 0.2 W m^{-2}$. This symmetry is achieved by increased reflection from SH clouds offsetting precisely the greater reflection from the NH land masses.

(Stephens et al. 2015)

The First Annual Mean Albedo from Satellite Observation



(Lewis et al. 2010)



Annual mean global albedo = 0.30

Hemispheric view from horizon to horizon

Measurements of solar radiation and that reflected from the Earth

1962-1965, Suomi's B&W radiometer onboard TIROS and ESSA satellites,

1966, MRIR onboard Nimbus-2, 1962-1966 in total 39 months

(Vonder Haar and Suomi 1969, 1971)

The First Annual Mean Albedo from Satellite Observation

TABLE 2. Mean annual radiation budgets of the entire earth-atmosphere system, the Northern Hemisphere and the Southern Hemisphere, as measured from first generation meteorological satellites together with first results from the second generation spacecraft. (The latter were weighted into the average as shown in Table 1.) A solar constant of $1.95 \text{ cal cm}^{-2} \text{ min}^{-1}$ was used in the evaluation.

	Planetary albedo (%)			Infrared loss ($\text{cal cm}^{-2} \text{ min}^{-1}$)			Net radiation ($\text{cal cm}^{-2} \text{ min}^{-1}$)		
	Northern Hemisphere	Southern Hemisphere	Global	Northern Hemisphere	Southern Hemisphere	Global	Northern Hemisphere	Southern Hemisphere	Global
First generation satellites*	29	29	29	0.33	0.33	0.33	+0.01	+0.01	+0.01
Second generation satellites**	30	30	30	0.33	0.34	0.34	0.00	0.00	0.00

* March, April, May 1962 and June 1963–November 1965 (33 months).

** First generation satellites plus Nimbus II and ESSA III (39 months, 1962–66).

TABLE 3. Radiative properties of the various bolometric coatings. The “W” refers to a high reflectivity/low emissivity response to the radiation (visible or infrared), and the “B” refers to a low reflectivity/high emissivity response to the radiation.

Coatings	Tabor	Gold	Black	White
Response to visible	B	W	B	W
Response to thermal infrared	W	W	B	B

(Nimbus-2)

MRIR (Medium Resolution Infrared Radiometer)

5-channel radiometer with 55km resolution

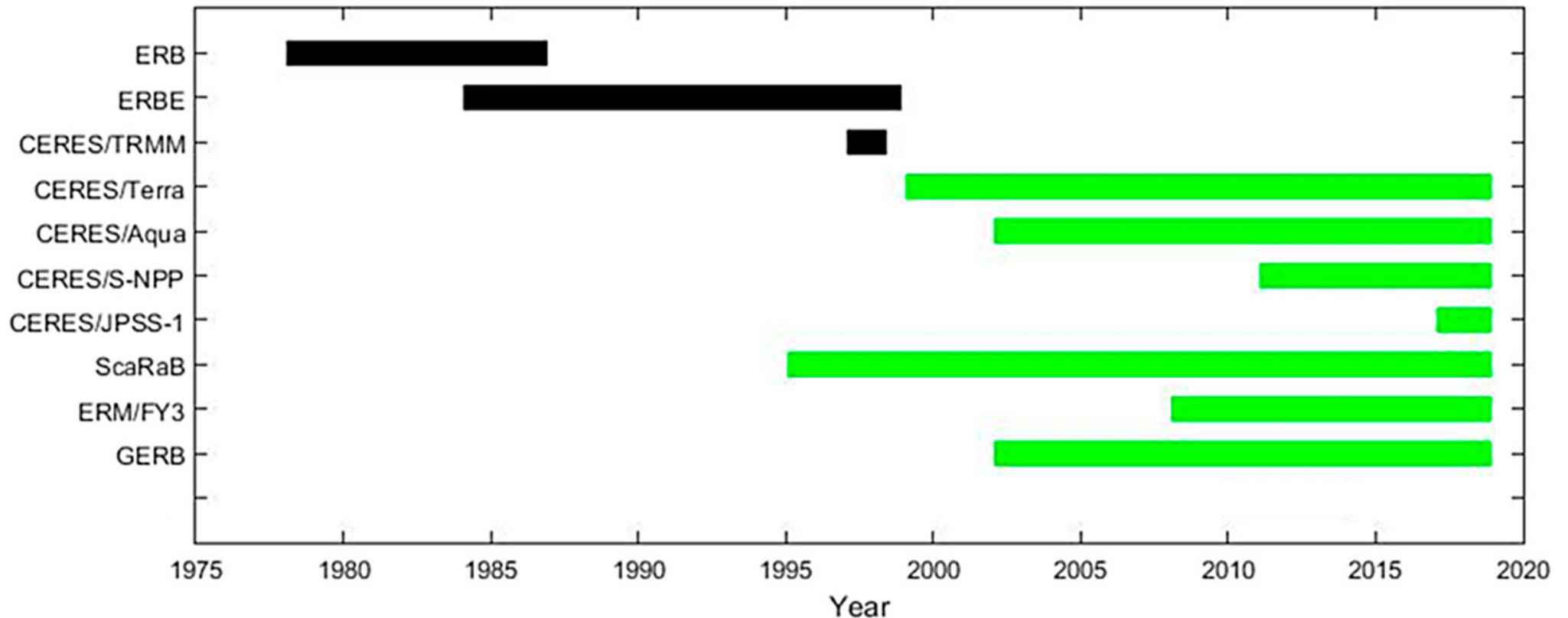
0.2~4.0 μm , 5~30 μm ,

6.4~6.9 μm , 10~11 μm , 14~16 μm .

Cross-track swath: 3000km

(Vonder Haar and Suomi 1971, Lewis et al. 2010)

Recent Satellite Observations of Earth's Radiation Budget



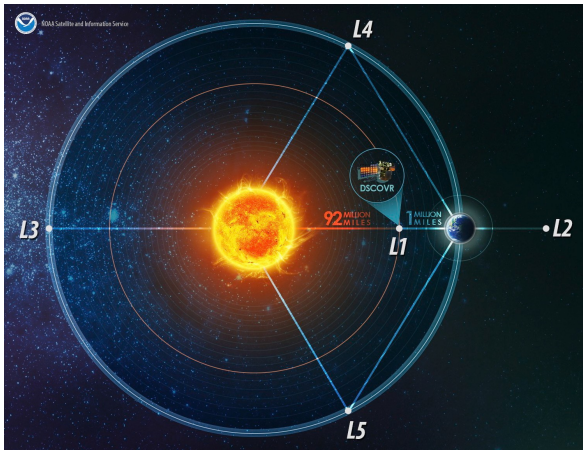
ERB: Earth Radiation Budget instrument, ERBE: Earth Radiation Budget Experiment,
CERES: Clouds and the Earth's Radiant Energy System, ScaRaB: Scanner for Radiation Budget,
ERM: Earth Radiation Measurement instrument, GERB: Geostationary Earth Radiation Budget,

(Liang et al. 2019)

Current Satellite Observations of Earth's Radiation Budget

- CERES/Terra, Aqua, S-NPP, NOAA-20
 - Clouds and the Earth's Radiant Energy System (CERES) was developed following ERB/Nimbus-7 (1978), ERBE/NOAA-9 (1984), etc.
 - Broadband but narrow angle sensor which needs Angular Distribution Models.
- ScaRaB
 - The Scanner for Radiation Budget (ScaRaB), jointly developed by France, Russia, Germany and India, ended in 2022
- GERB/MSG
 - Geostationary Earth Radiation Budget (GERB) onboard Meteosat Second Generation (MSG) satellites 1~4.
- EPIC/DSCOVR
 - Enhanced Polychromatic Imaging Camera (EPIC) onboard Deep Space Climate Observatory (DSCOVR) in Lagrange-1 point.
- Others
 - Estimation of upward SW irradiance from narrowband sensors, e.g. ISCCP

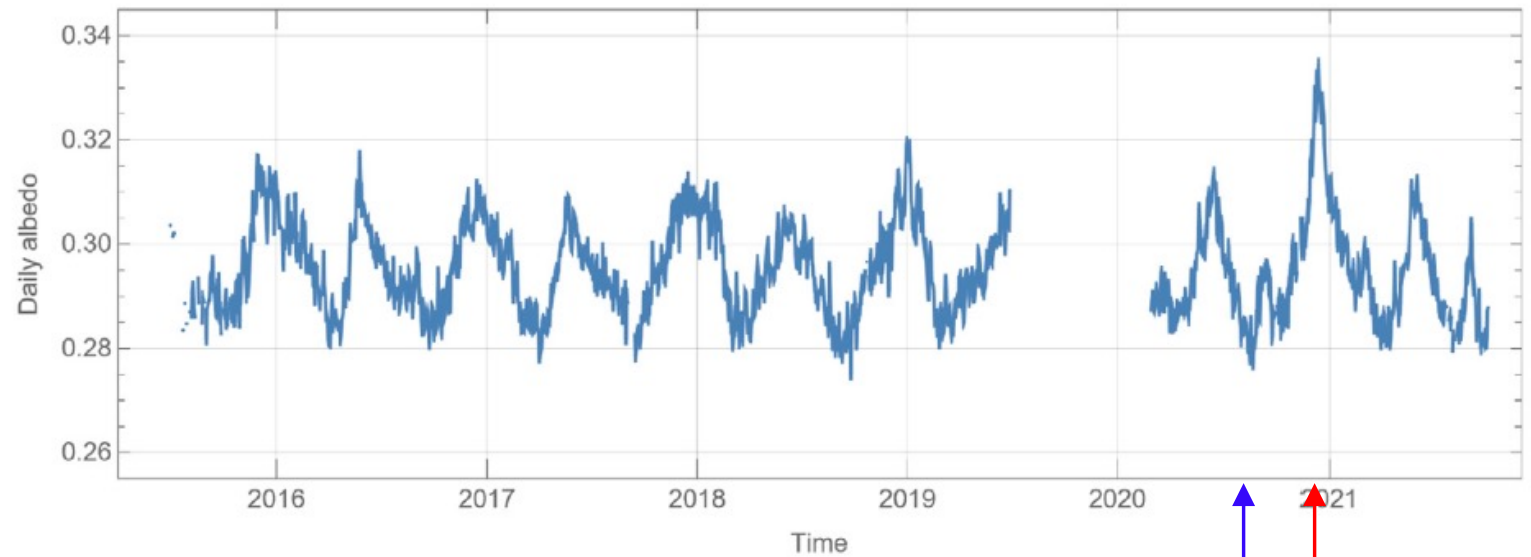
Daily Average of Earth's Albedo by EPIC/DSCOVR



Earth Polychromatic Imaging Camera (EPIC) onboard Deep Space Climate Observatory (DSCOVR)

Orbit : Lagrange-1 point (L1)

317, 325, 340, 388, 443, 551, 680, and 780 nm
→300~5000nm (broad band)
Radiance→Flux

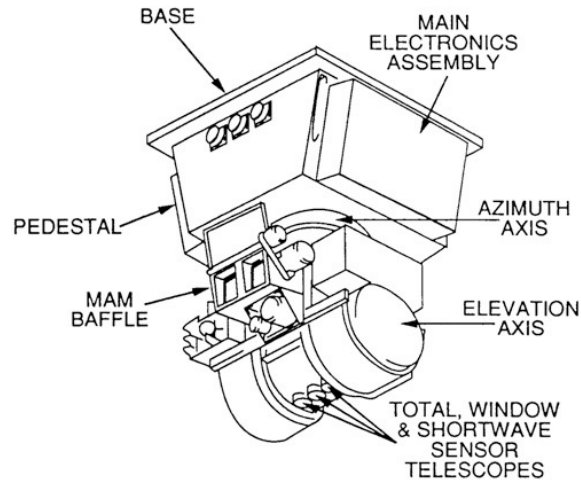


4 August 2020 (left)
13 December 2020 (right) :
Exceptional maximum in
the amount of shallow
convective clouds over the
subtropical Indian Ocean
and the Pacific east of
Australia

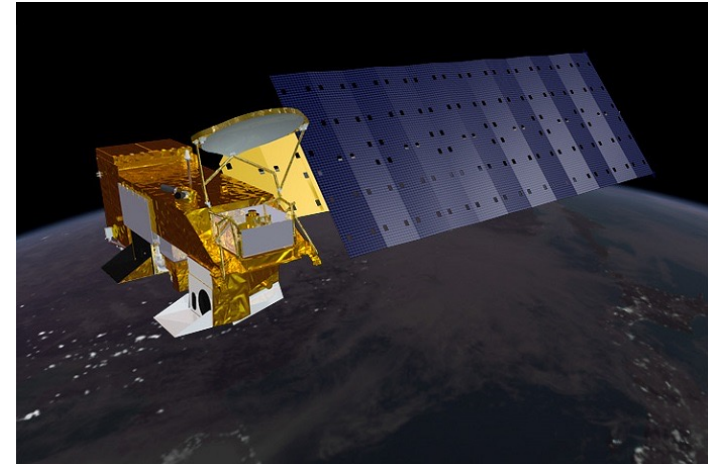
(Penttila et al. 2022)



Clouds and the Earth's Radiant Energy System (CERES)



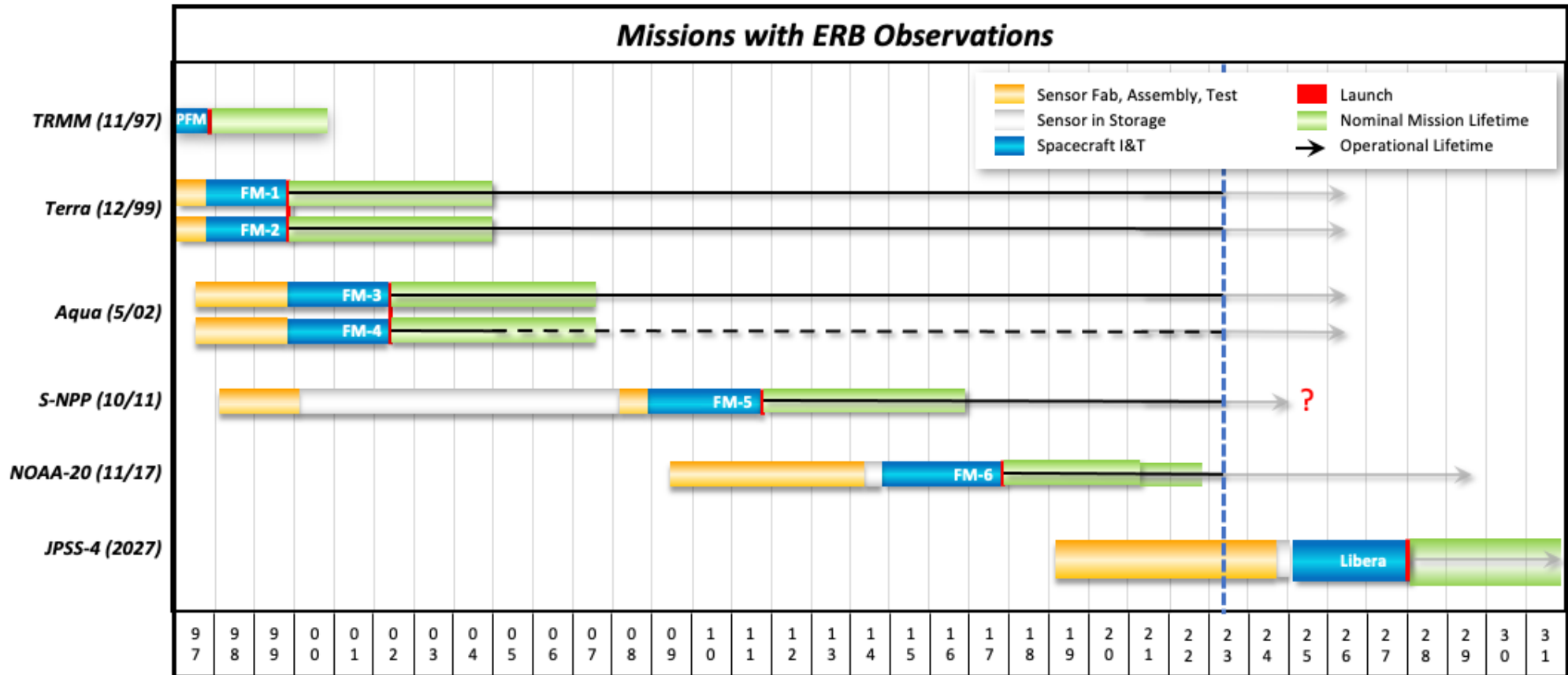
Aqua



Category	Instrument Characteristics
Spectral Range	0.3-5 μm (SW); 0.3-200 μm (TOT); 8-11 μm (WN; PFM, FM1-FM5); 0.3-35 μm (LW; FM6)
Field-of-View (equivalent diameter @ nadir)	10 km (PFM); 20 km (FM1-FM4); 24 km (FM5-FM6)
Geographic Coverage	Global daily
Angular Sampling	Fixed Azimuth Plane (crosstrack); Rotating Azimuth Plane; Programmable Azimuth Plane
Radiometric Accuracy	1% (SW) k=1; 0.5% (LW) k=1; 0.5% (TOT) k=1
Radiometric Stability	0.3%/decade k=1
Radiometric Precision	$< 0.3 \text{ Wm}^{-2} \text{ sr}^{-1} + 0.1\% \text{ of measured (SW)}$ $< 0.45 \text{ Wm}^{-2} \text{ sr}^{-1} + 0.1\% \text{ of measured (LW)}$ $< 0.2 \text{ Wm}^{-2} \text{ sr}^{-1} + 0.1\% \text{ of measured (TOT)}$

(CERES webpage)

CERES Flight Schedule



- Currently, 6 CERES instruments fly on 4 satellites: Terra (L1999), Aqua (L2002), SNPP(L2011), NOAA-20 (L2017)
- Libera scheduled for launch in 2027 on JPSS-4

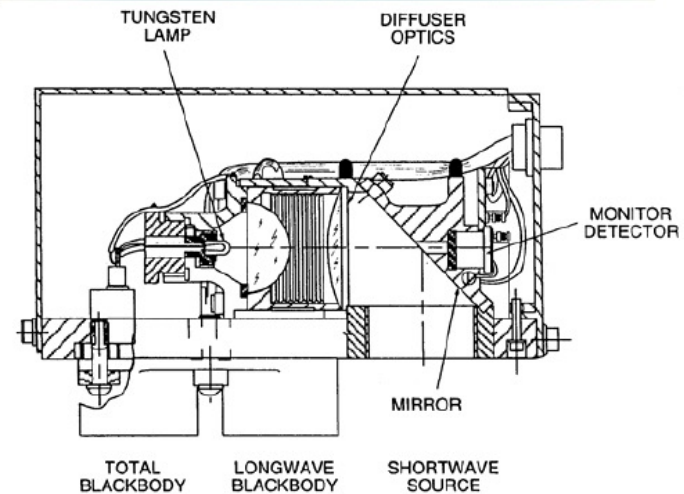
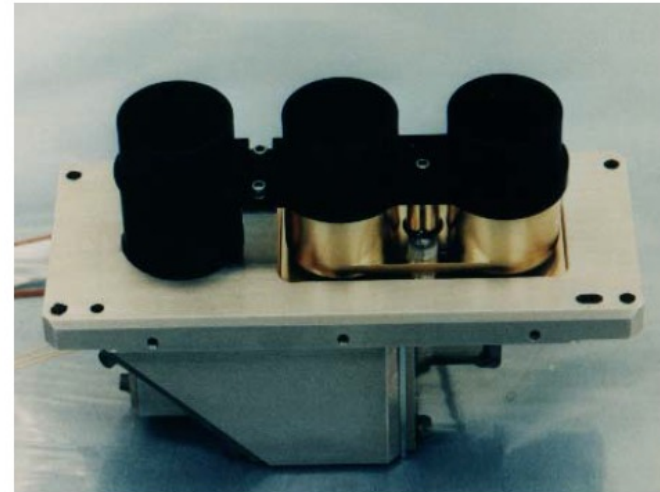
(CERES webpage)

CERES onboard Calibration Sources

Internal Calibration Module (ICM)

- Blackbodies for the Total and Window channels
- Temperature knowledge obtained via Platinum Resistance Thermometers (PRTs)
- Quartz-halogen tungsten lamp for the Shortwave channel
- ICM Provides 3 unique radiance levels for the SW and LW sources

(Priestley et al. CERES Data Products Workshop 2003)

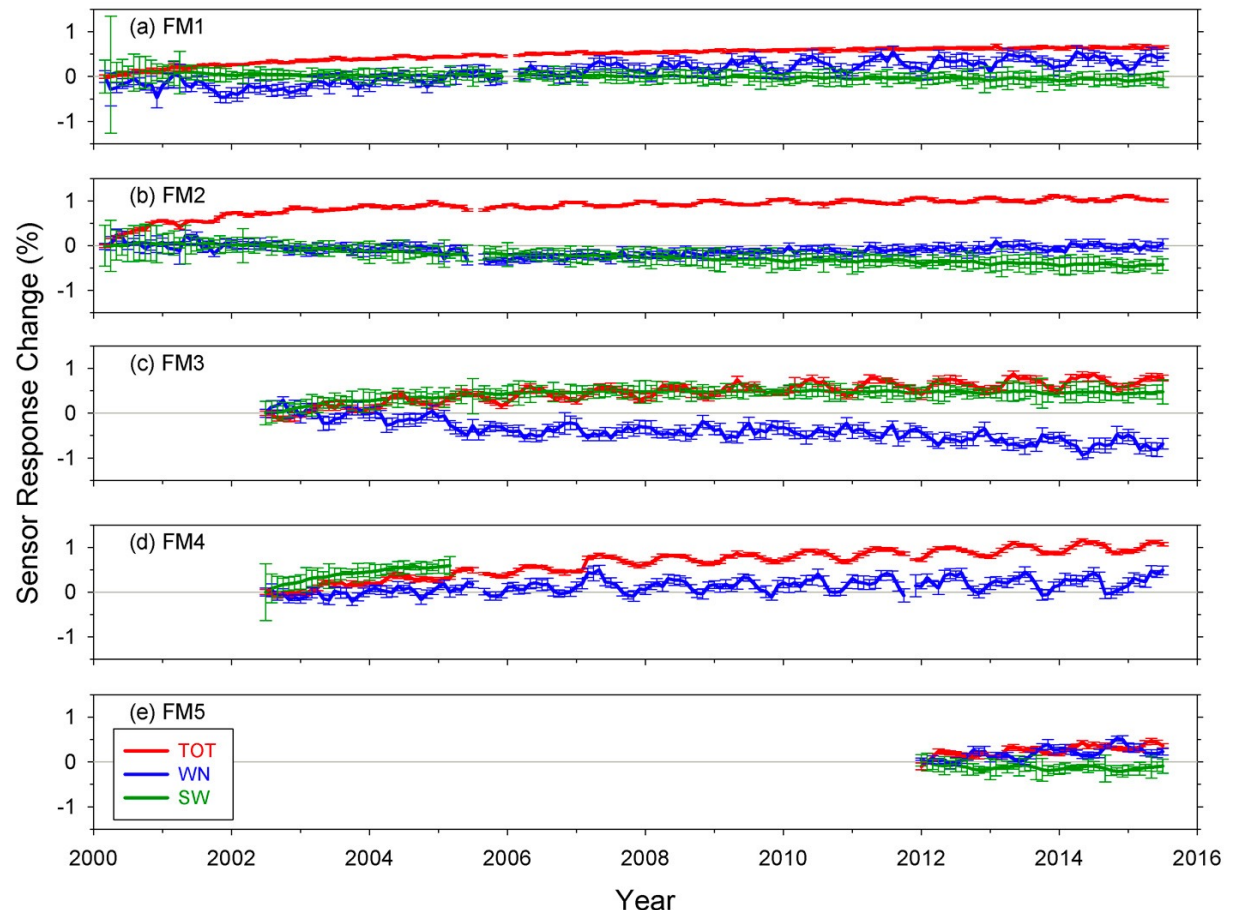


Degradation of CERES Radiometers

The Shortwave Internal Calibration Source (SWICS) consists of an evacuated quartz tungsten lamp operating at three discrete current levels producing spectra equivalent to 2100 K, 1900 K and 1700 K brightness temperatures.

The radiometers observe the Internal Calibration Module (ICM) in every normal cross-track elevation scan.

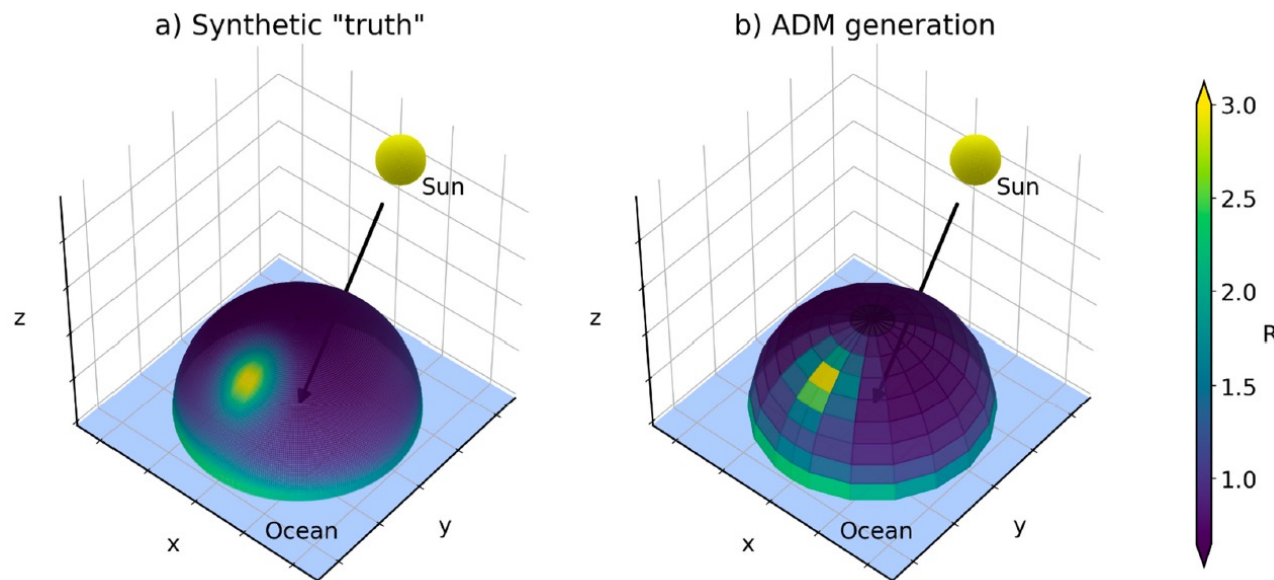
The Mirror Attenuator Mosaic (MAM) is a solar diffuser plate used for calibrating the shortwave sensor and the total sensor. It consists of a baffle to block stray light and a nickel substrate with aluminum coated spherical divots that attenuate and redirect the solar radiation into the field of view of the sensors.



On-orbit sensor gains for CERES FM1–FM5 instruments. The data span from March 2000–July (Loeb et al. 2016)

Angular Distribution Models (ADMs)

Surface Type	Cloud Thermodynamic Phase	Cloud Fraction (%)	Cloud Optical Depth
Ocean (336)	Liquid, ice	0.1–10, 10–20, 20–30, 30–40, 40–50, 50–60, 60–70, 70–80, 80–90, 90–95, 95–99.9, 99.9–100	0.01–1.0, 1.0–2.5, 2.5–5.0, 5.0–7.5, 7.5–10, 10–12.5, 12.5–15, 15–17.5, 17.5–20, 20–25, 25–30, 30–40, 40–50, >50
Moderate–high tree/shrub coverage (60), low–moderate tree/shrub coverage (60), dark desert (60), bright desert (60)	Liquid, ice	0.1–25, 25–50, 50–75, 75–99.9, 99.9–100	0.01–2.5, 2.5–6, 6–10, 10–18, 18–40, >40



(Gristey et al. 2021)

Estimation of Broadband Radiation from Narrowband Data

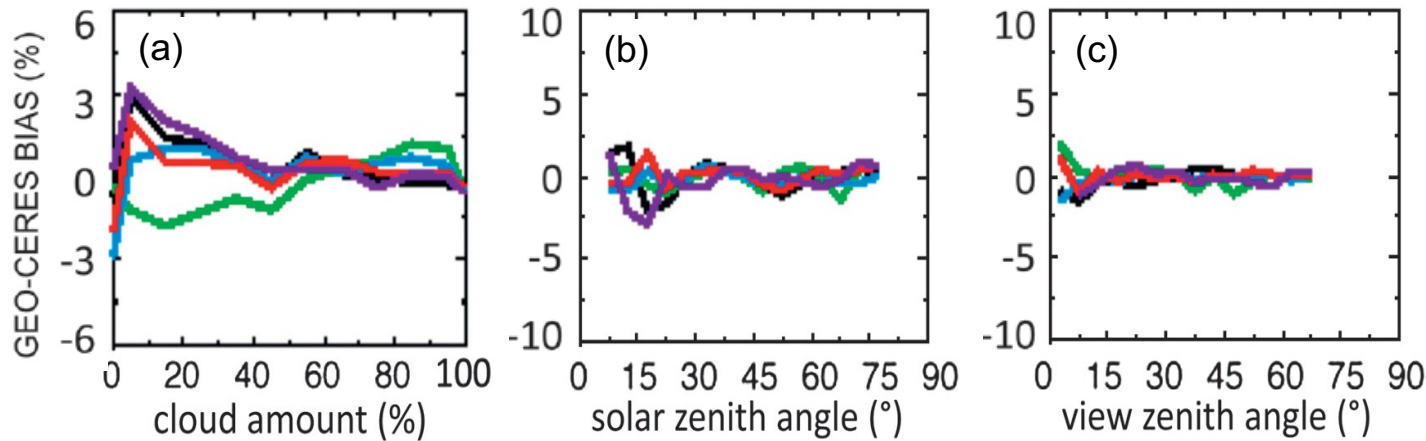
	Shortwave narrowband-to-broadband regressions
MODIS spectral channels (μm)	0.47, 0.65, 0.86, and 1.63 (<i>Terra</i>) or 2.13 (<i>Aqua</i>)
Surface types	Ocean, forests, savannas, grassland/crops, dark desert, bright desert, fresh snow, sea ice, and permanent snow (Greenland and Antarctica).
Viewing zenith angle	Seven bins from 0° to 70° in 10° increments.
Solar zenith angle	Nine bins from 0° to 90° in 10° increments.
Relative azimuth angle	Nine bins from 0° to 180° in 20° increments.

- Sun-Synchronous polar orbital satellite → Daytime observation once a day
- Geostationary satellite does not have a broadband radiometer (except for GERB/Meteosat)
- Estimation of broadband radiation using narrowband radiometer data
- CERES and MODIS are on board Terra and Aqua
- Application of CERES/MODIS method to geostationary satellite

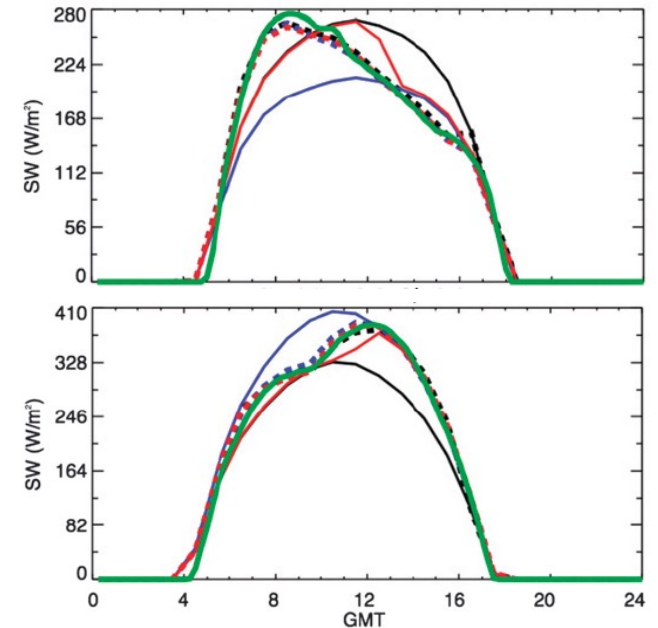
(* MODIS : Moderate-Resolution Imaging Spectroradiometer)

Interpolation for Daily Average

GEO-derived BB-minus-CERES SW flux bias



(a) GEO-derived BB-minus-CERES SW flux bias for cloud amount, (b) SZA, and (c) viewing zenith angle for January 2001 over the Meteosat-7 (black), Meteosat-5 (green), GMS-5 (cyan), GOES-10 (red), and GOES-8 (purple) domains.



Monthly hourly CERES and GERB flux comparison for January 2005. (top) maritime stratus (20.58S, 10.58E), (bottom) land convection (20.58S, 20.58E) region. Black, blue, and red lines represent Terra, Aqua, and Terra1Aqua datasets, respectively. Solid and dotted lines represent the CO and CG methods, respectively. GERB is the thick green line.

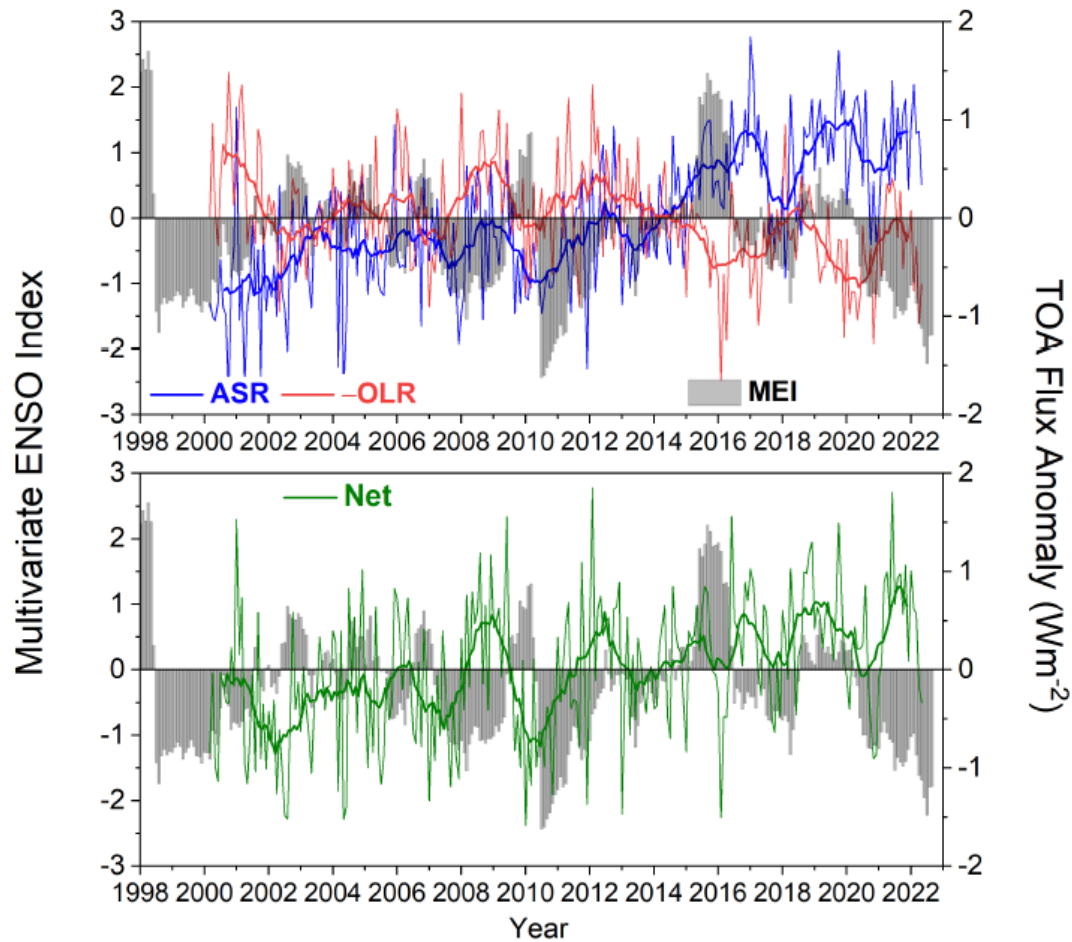
Uncertainty in $1^\circ \times 1^\circ$ monthly ~ 2.5 (W/m²) for all sky, 5 (W/m²) for clear sky
(Instrument calibration, radiance-to-flux conversion error and diurnal corrections)

(Doelling et al. 2013, and CERES webpage)

Variation in the Radiation Budget at TOA

Global Mean All-Sky TOA Flux Anomalies & Multivariate ENSO Index
(CERES EBAF Ed4.2; 03/2000–05/2022)

(Loeb CERES STM 2022)



EBAF Trends (03/2000-05/2022)

ASR: 0.70 ± 0.20 Wm⁻² per decade

LW: -0.28 ± 0.20 Wm⁻² per decade

NET: 0.42 ± 0.19 Wm⁻² per decade

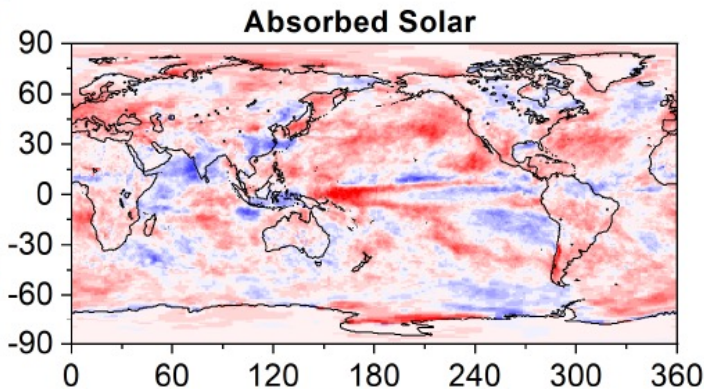
Trends of Radiation Budget at TOA and SST

TOA Radiation Changes (03/2000 – 05/2022)

Hemis. Trends
($\text{Wm}^{-2} \text{dec}^{-1}$)

NH: 0.78 ± 0.24

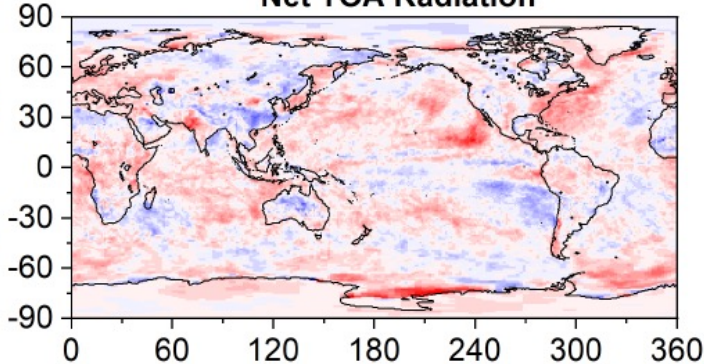
SH: 0.62 ± 0.24



Net TOA Radiation

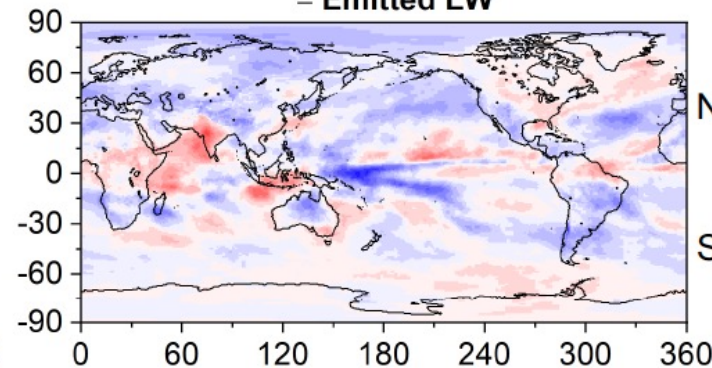
NH: 0.46 ± 0.22

SH: 0.39 ± 0.27

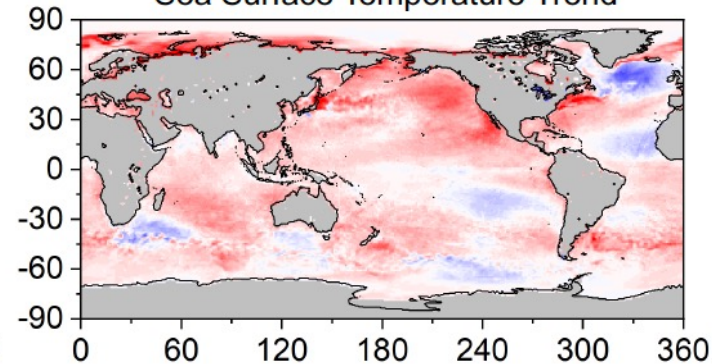


($\text{Wm}^{-2} \text{dec}^{-1}$)

- Emitted LW



Sea Surface Temperature Trend



(K dec^{-1})

Hemis. Trends
($\text{Wm}^{-2} \text{dec}^{-1}$)

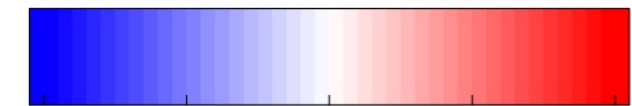
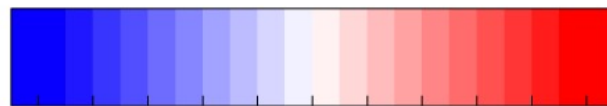
NH: -0.32 ± 0.22

SH: -0.24 ± 0.23

Downward
Positive

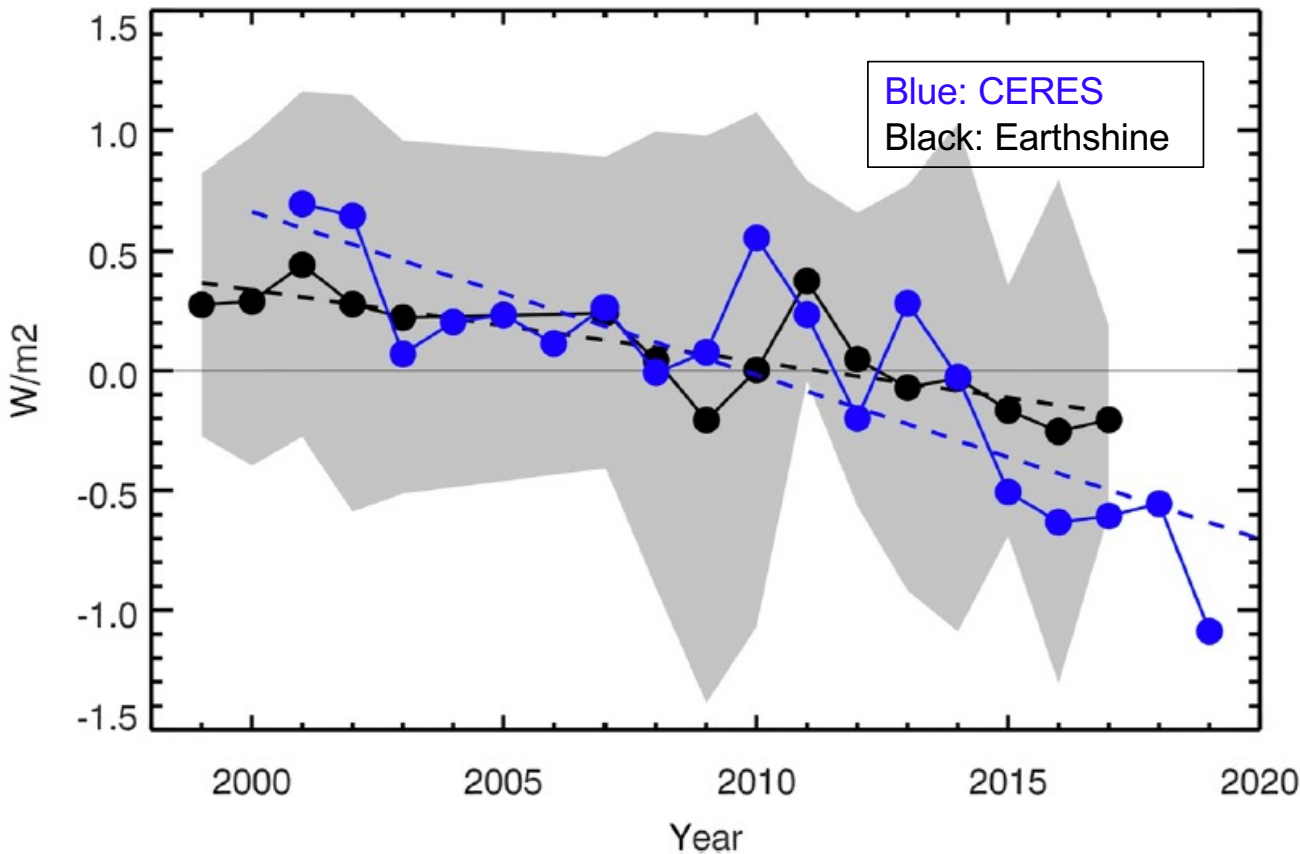
SST: ERA5

Radiation:
CERES satellite obs.
(Downward positive)

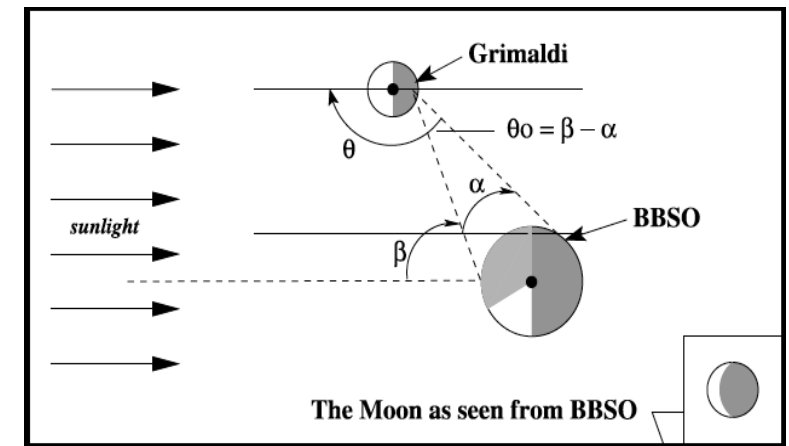


(Loeb CERES STM 2022)

Comparison between CERES and Earthshine



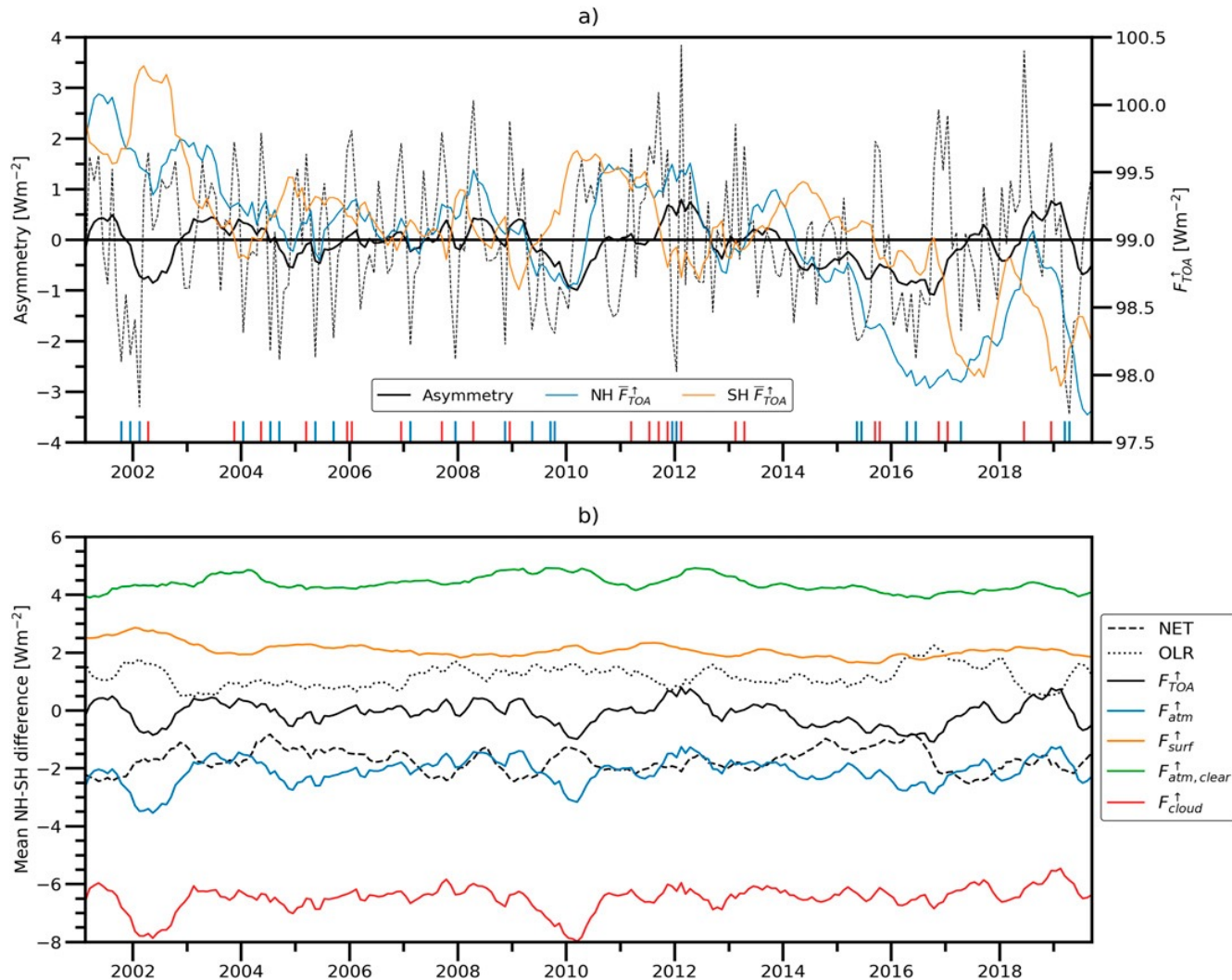
Global albedo can be determined by measuring the amount of sunlight reflected from the Earth and in turn, back to the Earth from the dark portion of the face of the Moon. (Qiu et al. 2014)



BBSO : Big Bear Solar Observatory

(Goode et al. 2021)

Hemispheric Differences in Upward SW Radiation at TOA



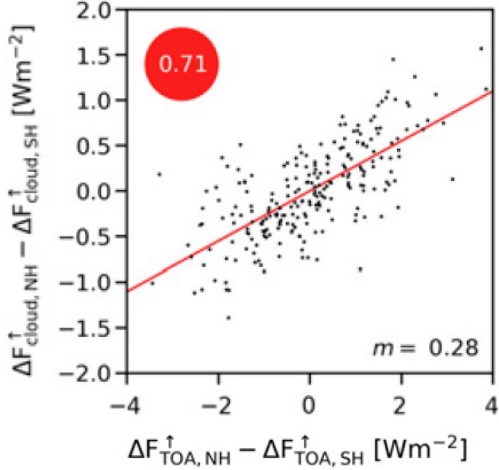
CERES EBAF Dataset (2001 ~ 2020)

- Very small difference between NH and SH
- Decreasing trend in both of NH and SH
- Contribution of clear sky atmosphere is larger in NH than SH → Aerosols?
- Contribution of cloud is larger in SH than NH
- Contribution of surface is larger in NH than SH → Snow and Ice

(Jonsson and Bender 2022)

Relationship between Individual Factors and Albedo Symmetry

Tropics (0°-20°)



Analyses are based on the monthly mean data.

Contribution of all-sky atmosphere

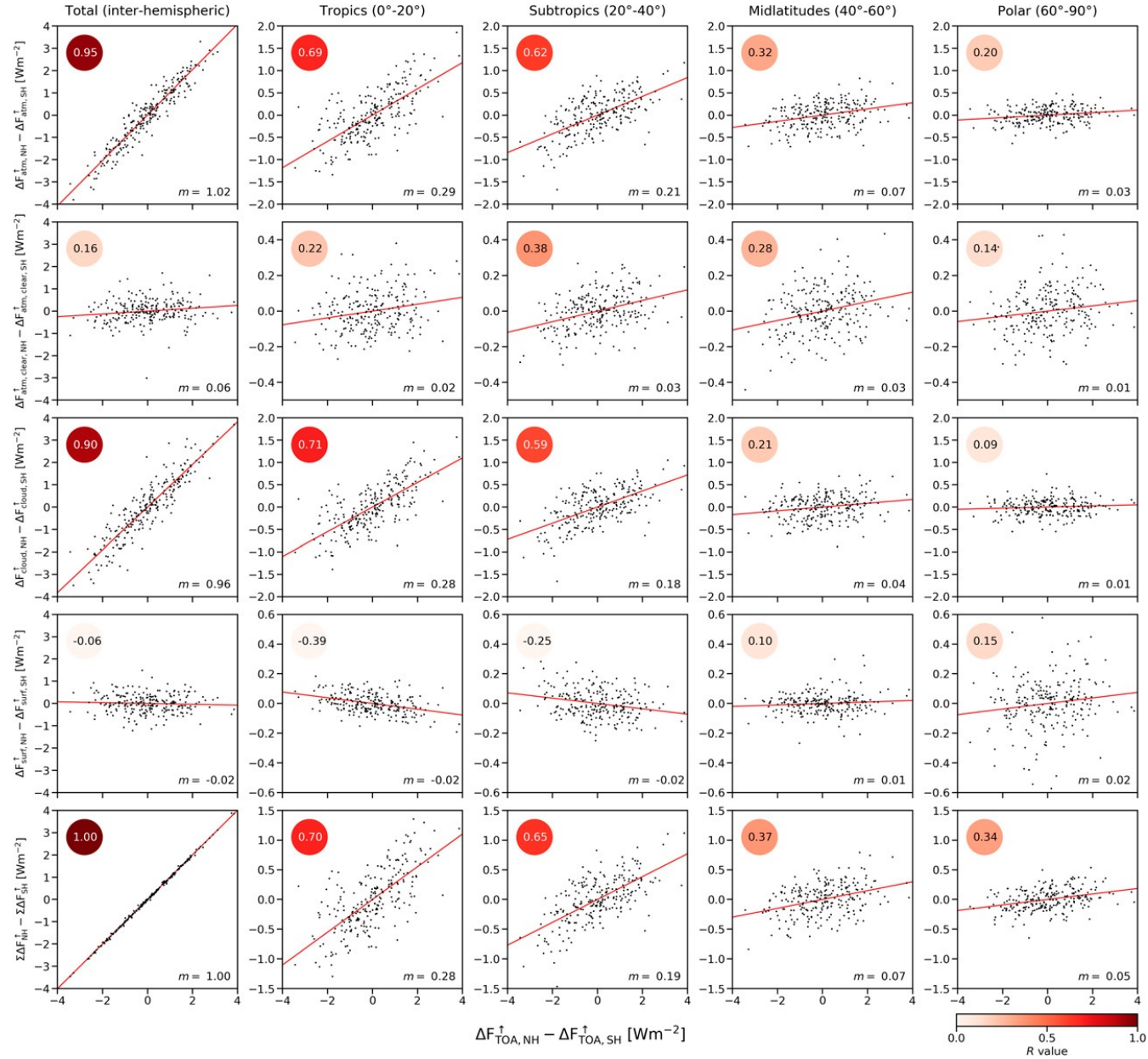
Contribution of clear-sky atmosphere

Contribution of cloud

Contribution of surface

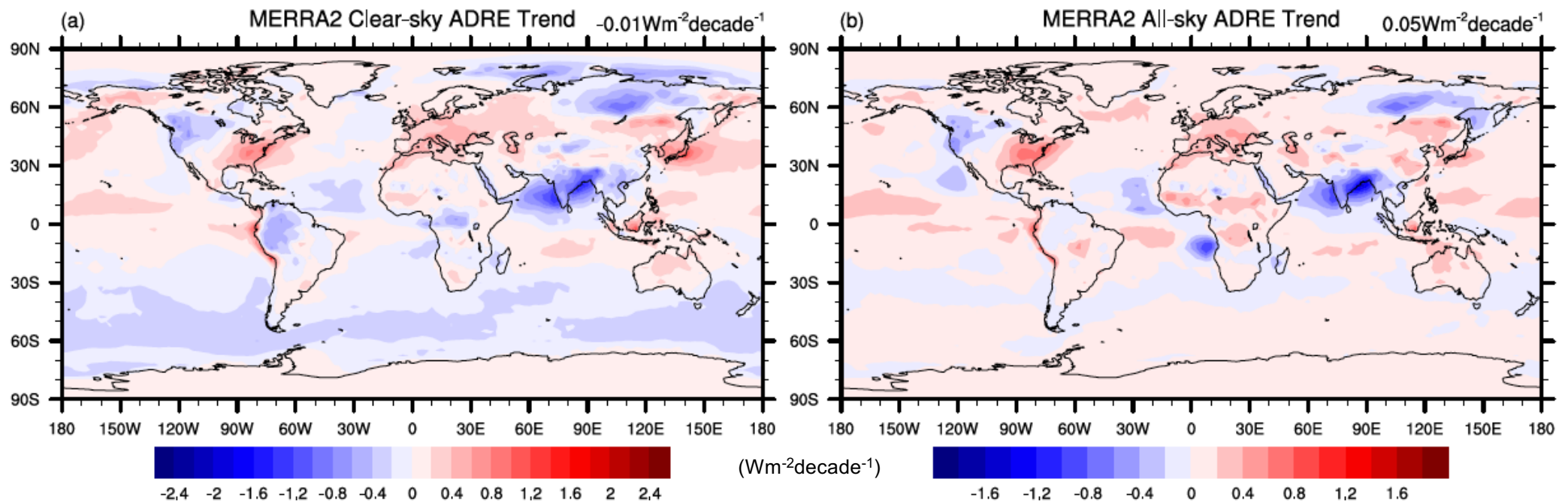
Total

(Jonsson and Bender 2022)



Discussion: Trend of Aerosol Direct Radiative Effect (2000-2021)

Aerosols do not contribute to the decreasing trend of albedo.



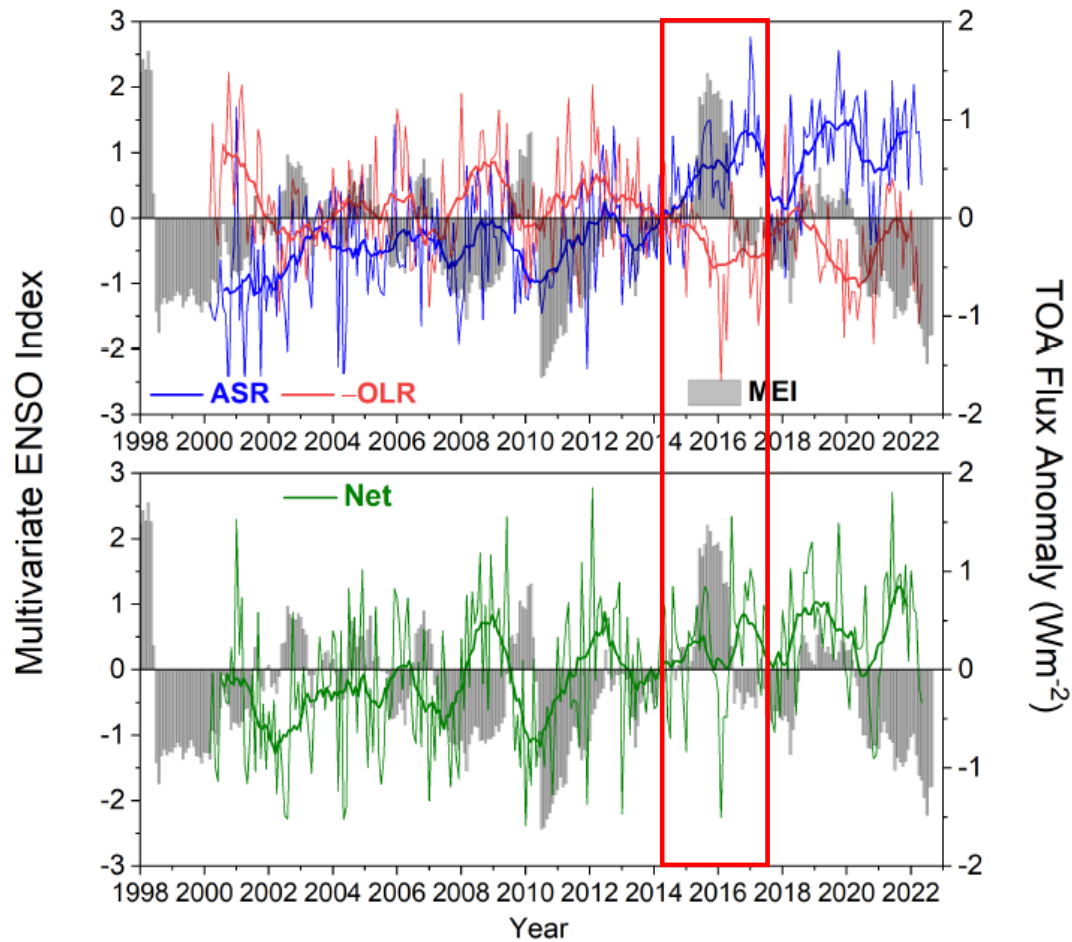
MERRA: Modern-Era Retrospective analysis for Research and Applications
(Reanalysis Data by NASA)

(Yu and Huang 2023)

Discussion : Variation in the Radiation Budget at TOA and El Nino, PDO

Global Mean All-Sky TOA Flux Anomalies & Multivariate ENSO Index
(CERES EBAF Ed4.2; 03/2000–05/2022)

(Loeb CERES STM 2022)



EBAF Trends (03/2000-05/2022)

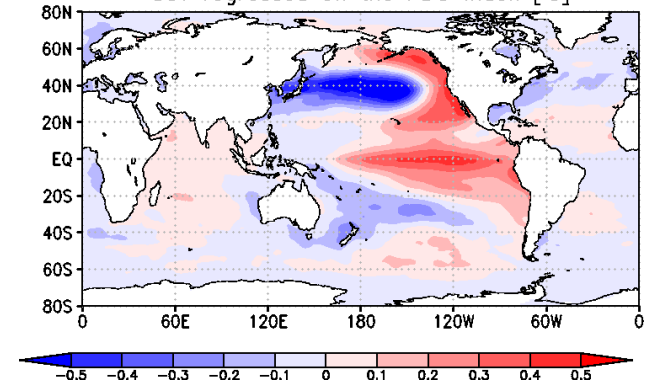
ASR: $0.70 \pm 0.20 \text{ Wm}^{-2}$ per decade

LW: $-0.28 \pm 0.20 \text{ Wm}^{-2}$ per decade

NET: $0.42 \pm 0.19 \text{ Wm}^{-2}$ per decade

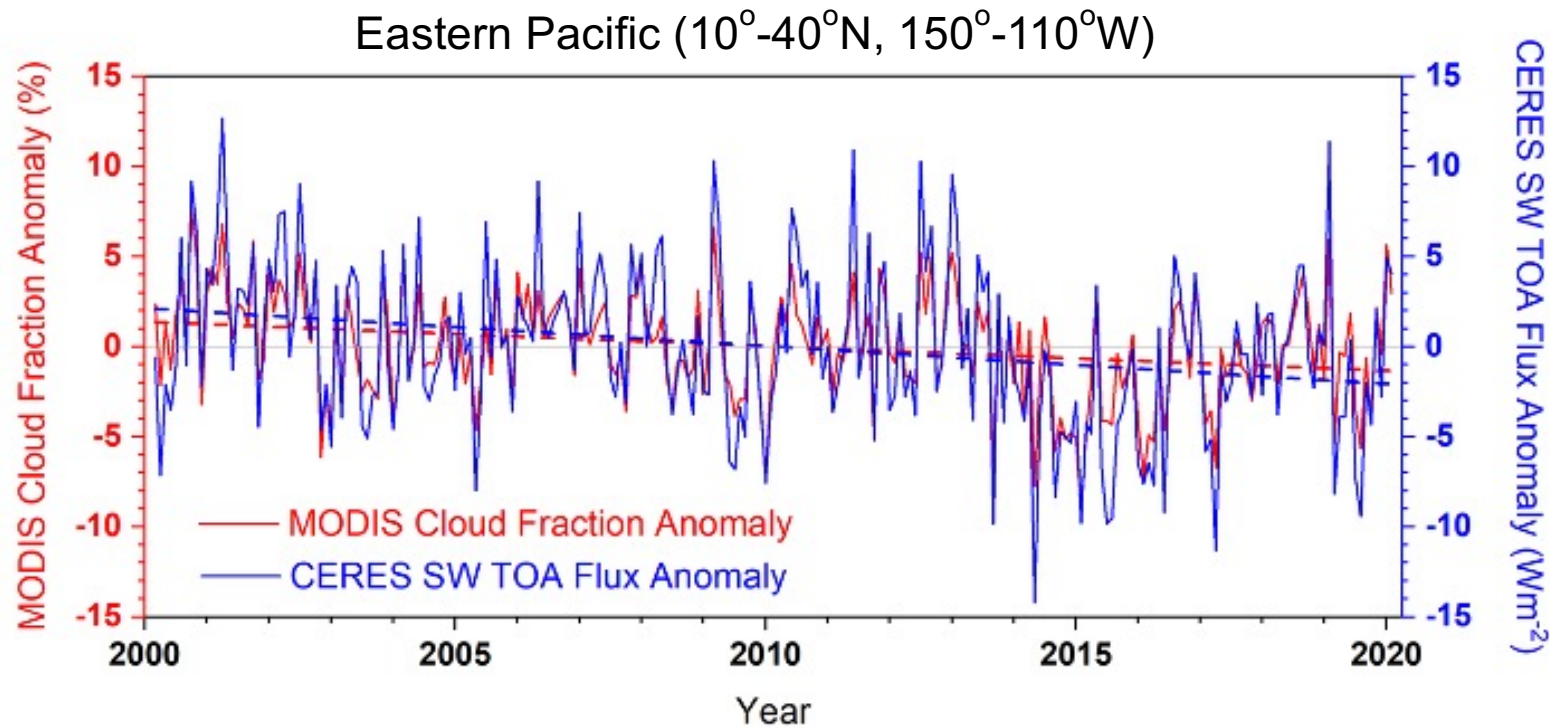
: PDO Index : Positive

SST regressed on the PDO index [$^{\circ}\text{C}$]



(JMA)

Discussion: Cloud Fraction and SW TOA Flux in Eastern Pacific



Trends

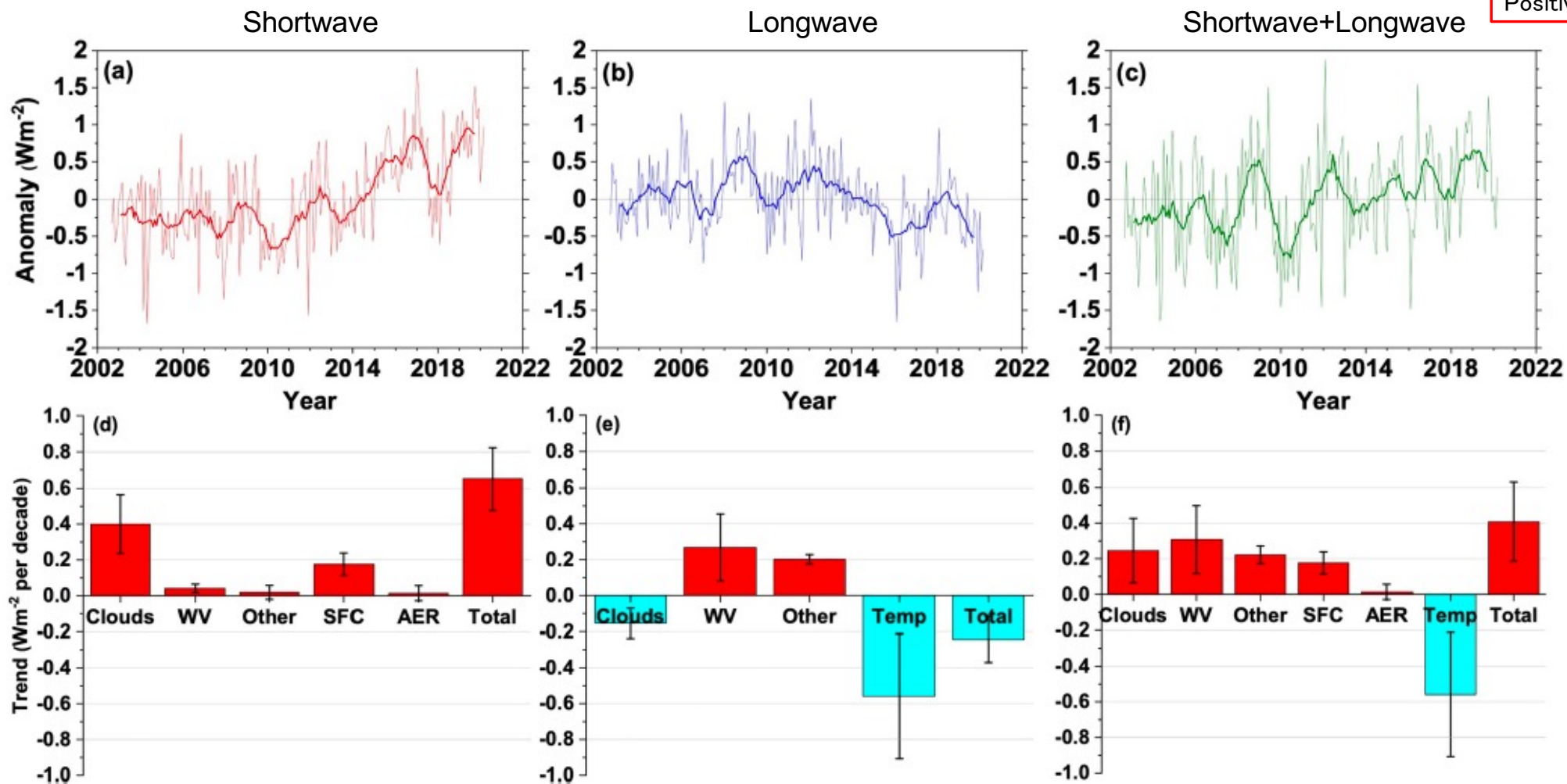
MODIS Cld frac: -1.4 ± 1.1 %/decade

CERES SW TOA: -2.1 ± 1.6 Wm^{-2} /decade

(Loeb et al. 2022)

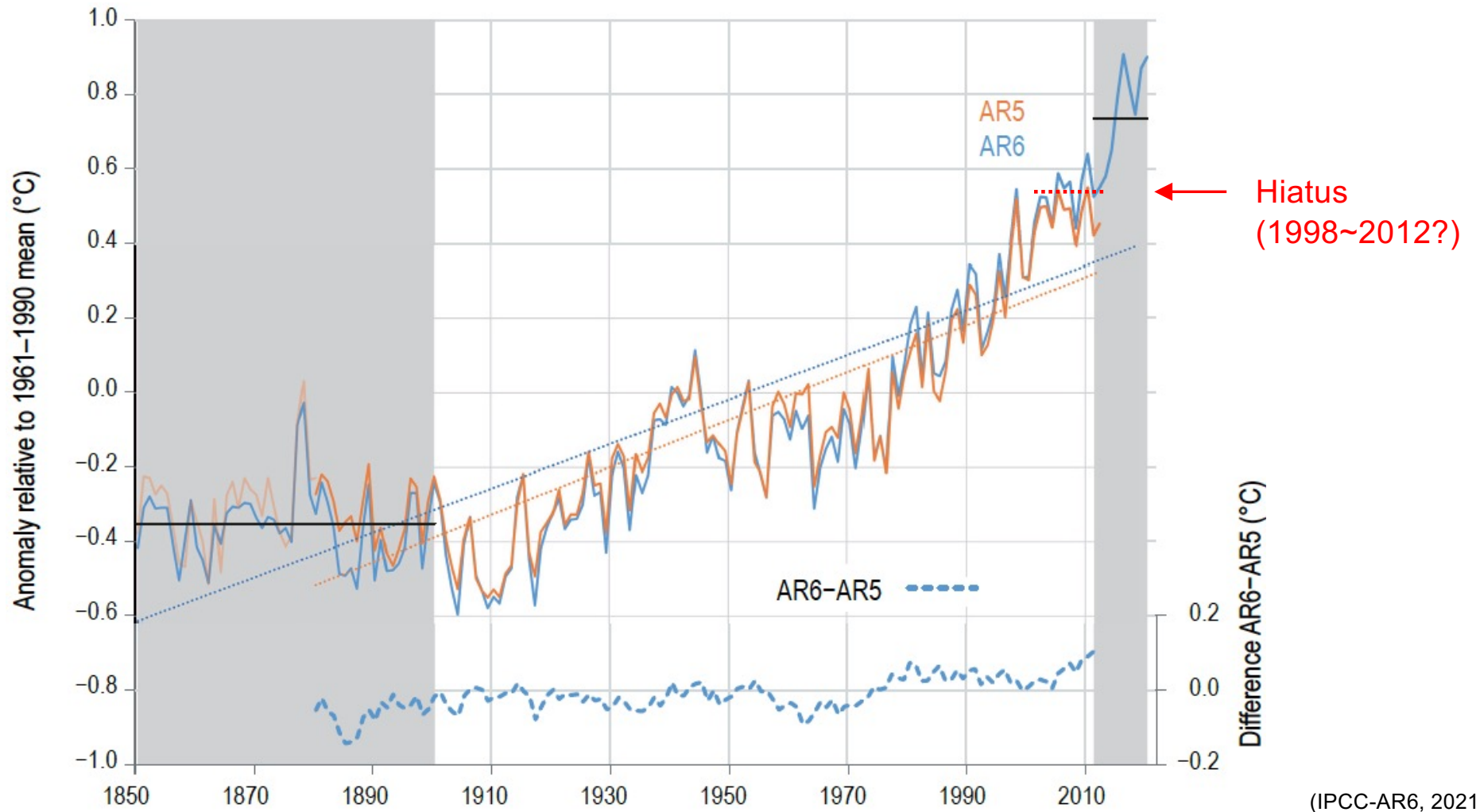
Discussion: Variations in the Radiation Budget at the top of the Atmosphere and Contributing Factors

Downward
Positive

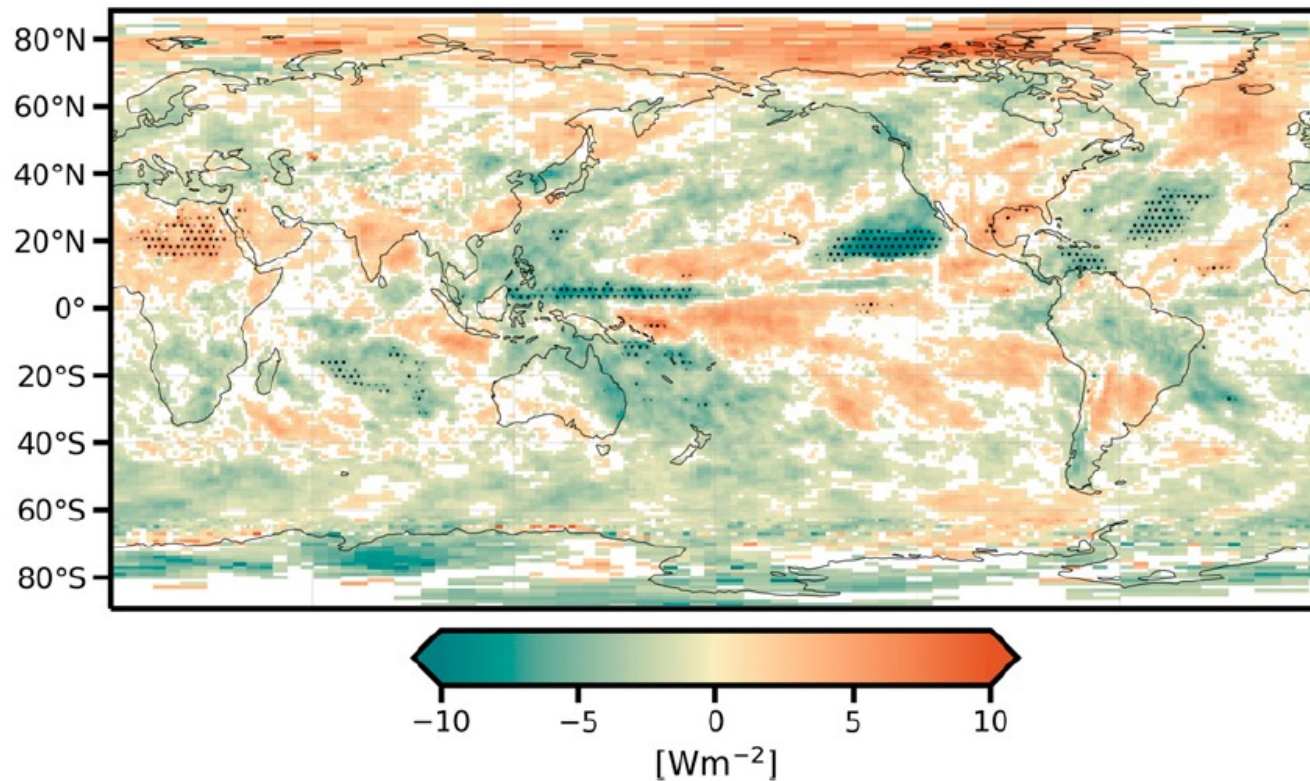


(Loeb et al. 2021)

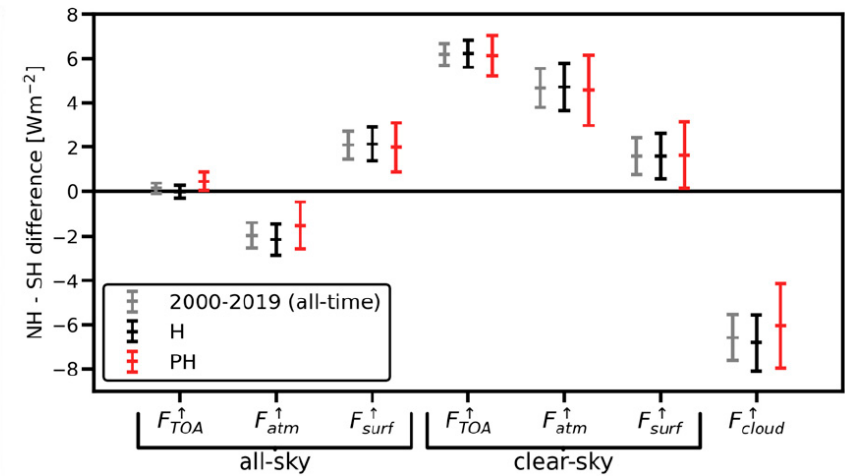
Discussion : Variation in the Global Surface Temperature



Discussion : Changes in the SW Radiation Budget at TOA due to Hiatus/Post Hiatus



Difference of Upward SW Radiation at TOA between PH and H (PH-H)



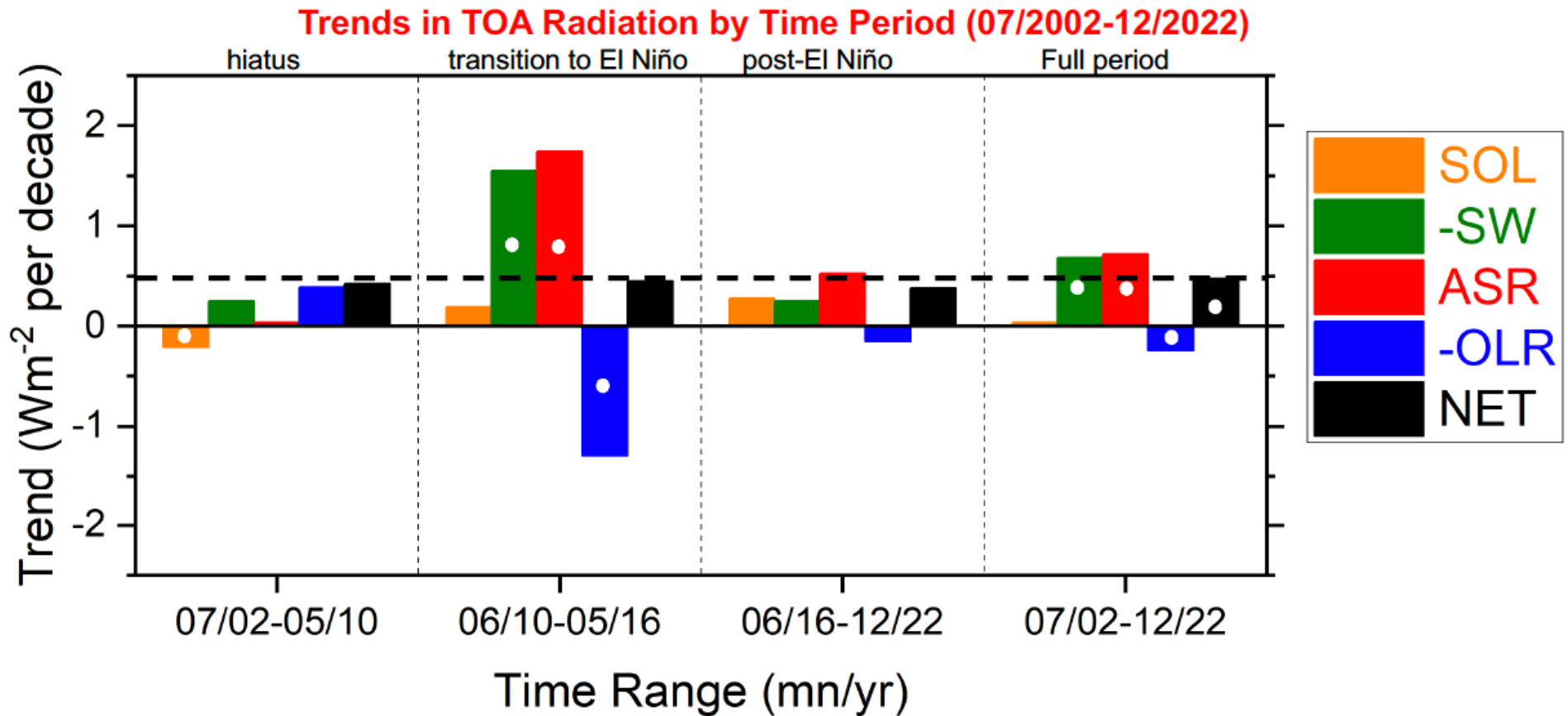
Hemispheric asymmetry of upward SW radiation for H, PH, and whole period

H: 2000-2013

PH: 2013-2019

(Jonsson and Bender 2022)

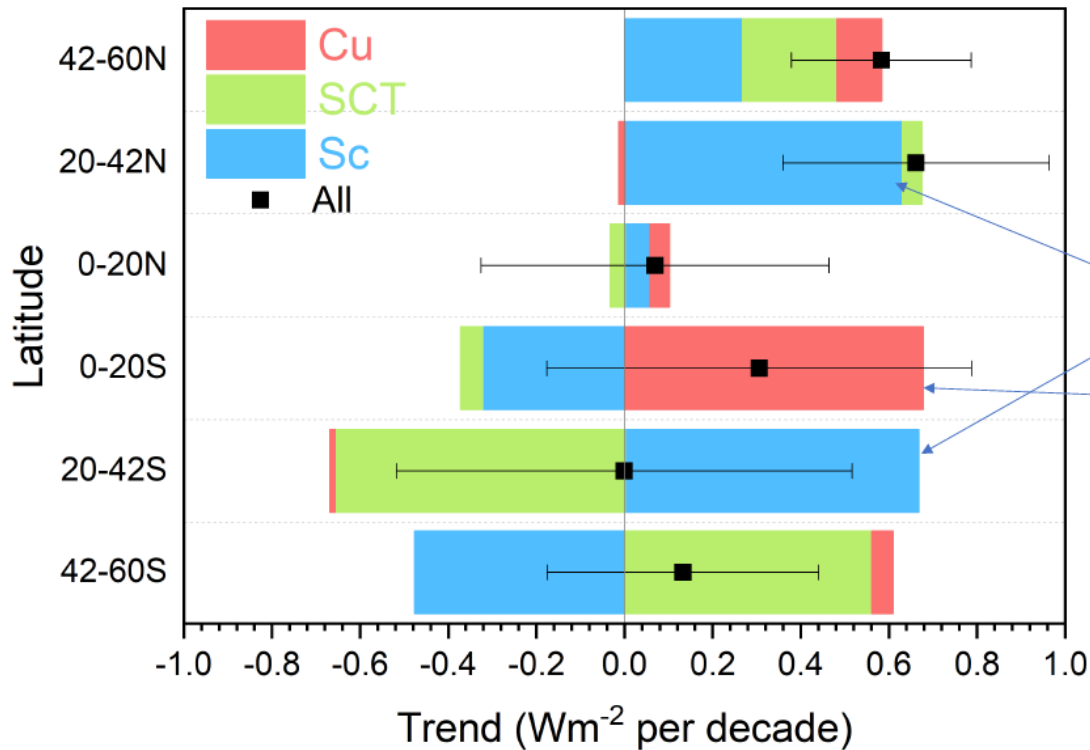
Discussion : Changes in the SW Radiation Budget at TOA Related to EL Nino and Hiatus/Post Hiatus



(Loeb CERES STM 2023)

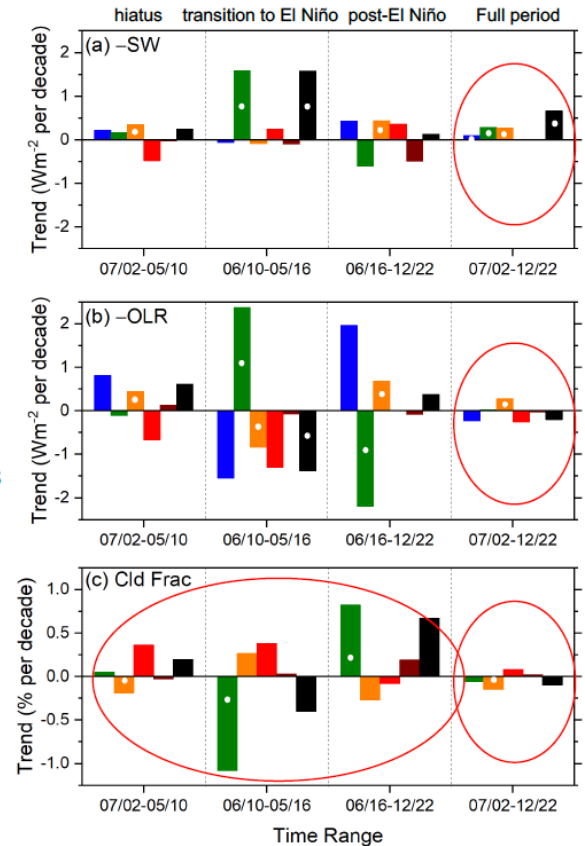
Discussion : Changes in the SW Radiation Budget at TOA Related to Clouds

Zonal ASR Trends by Low Cloud Type (07/2002–12/2022)



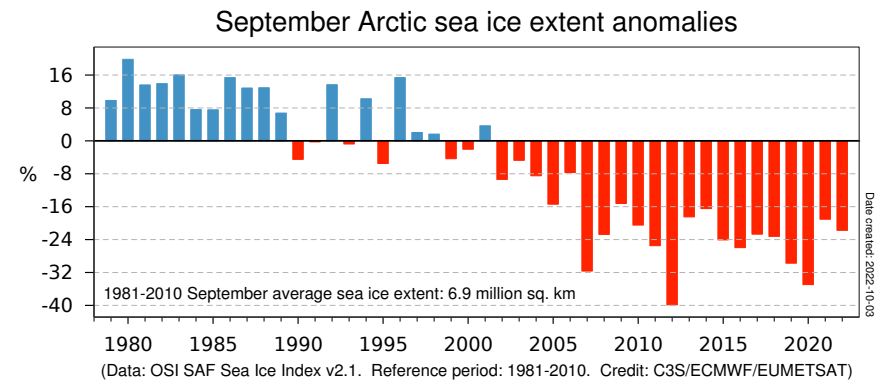
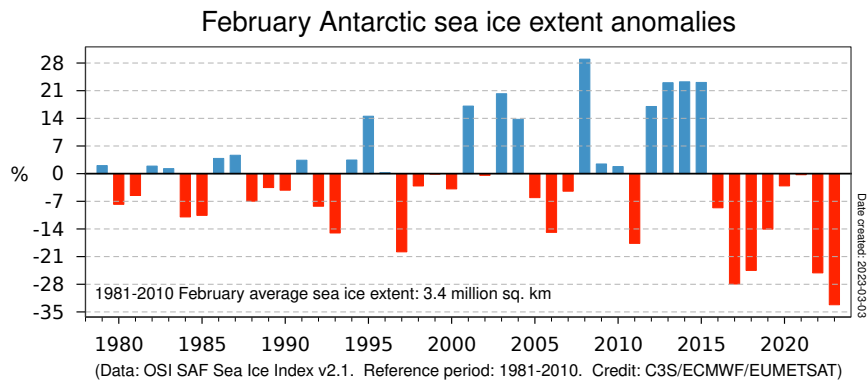
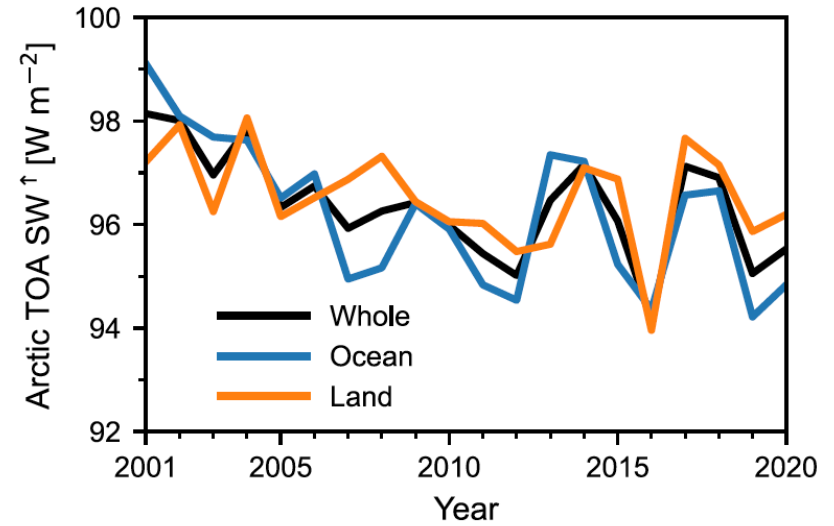
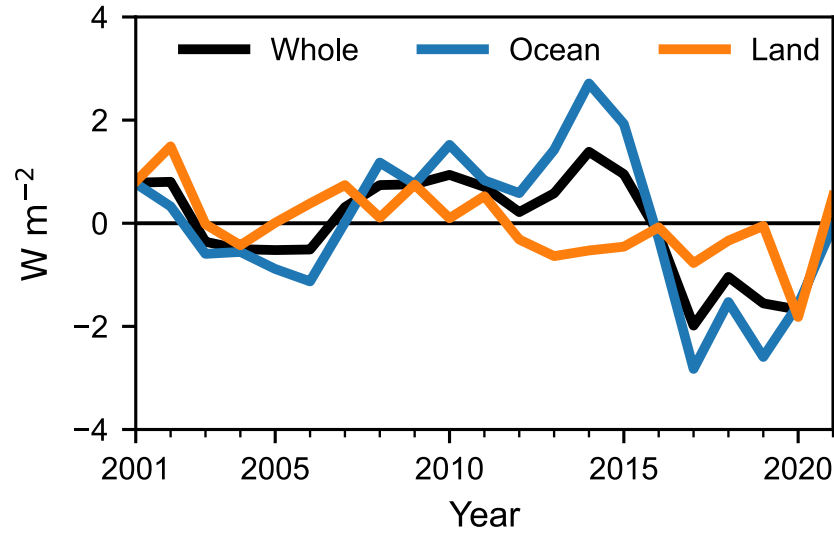
Reduction in Sc in NH and SH subtropics

Reduction in Cu in SH tropics

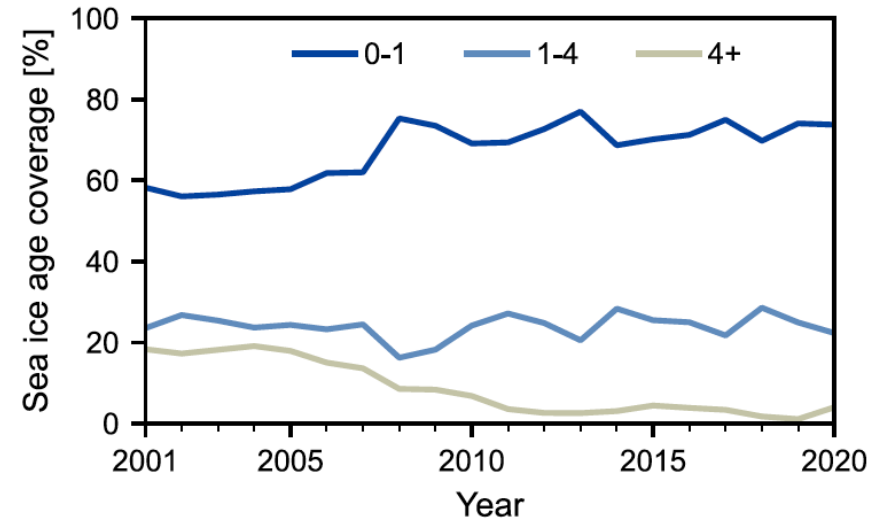
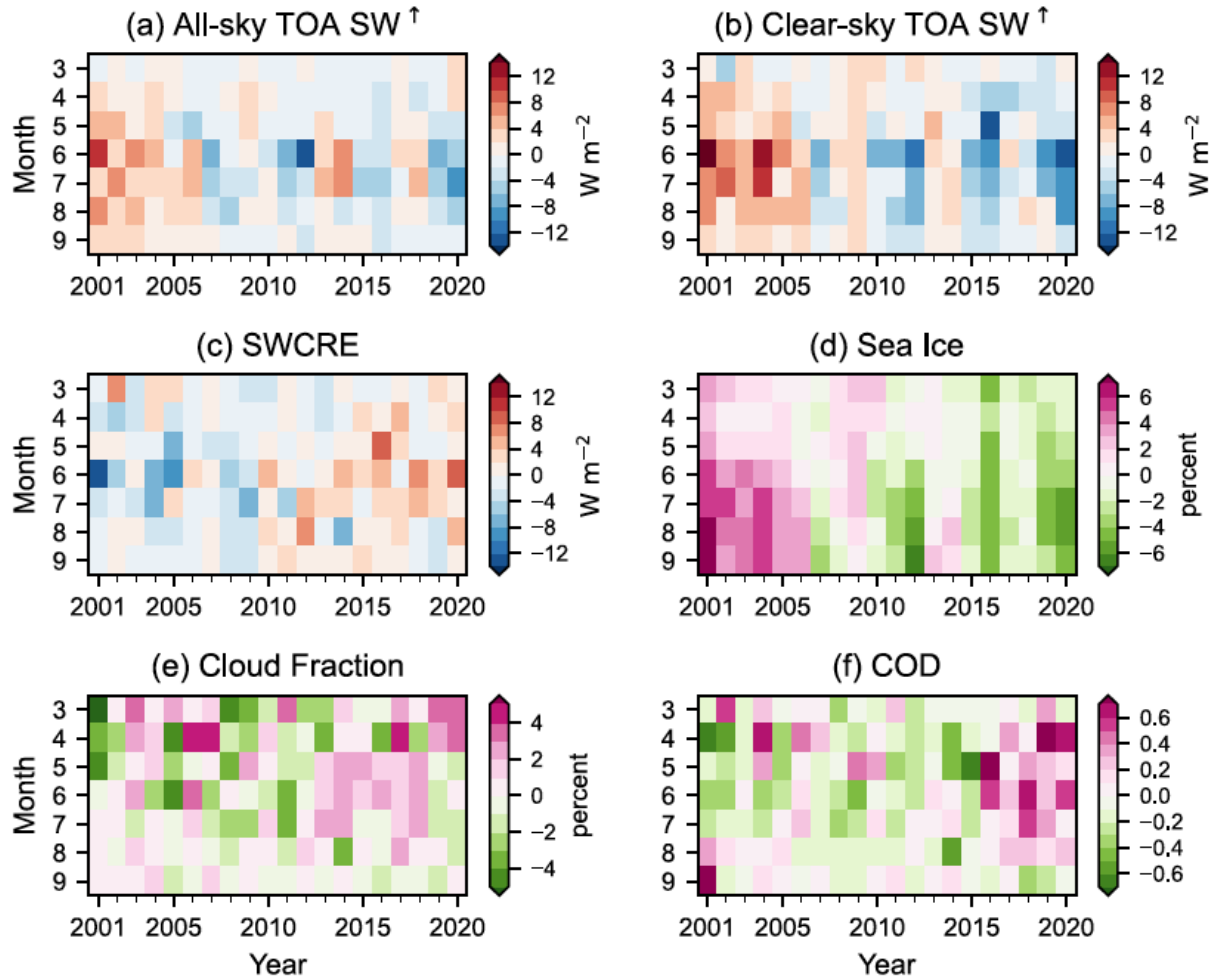


(Loeb CERES STM 2023)

Discussion : Antarctic and Arctic



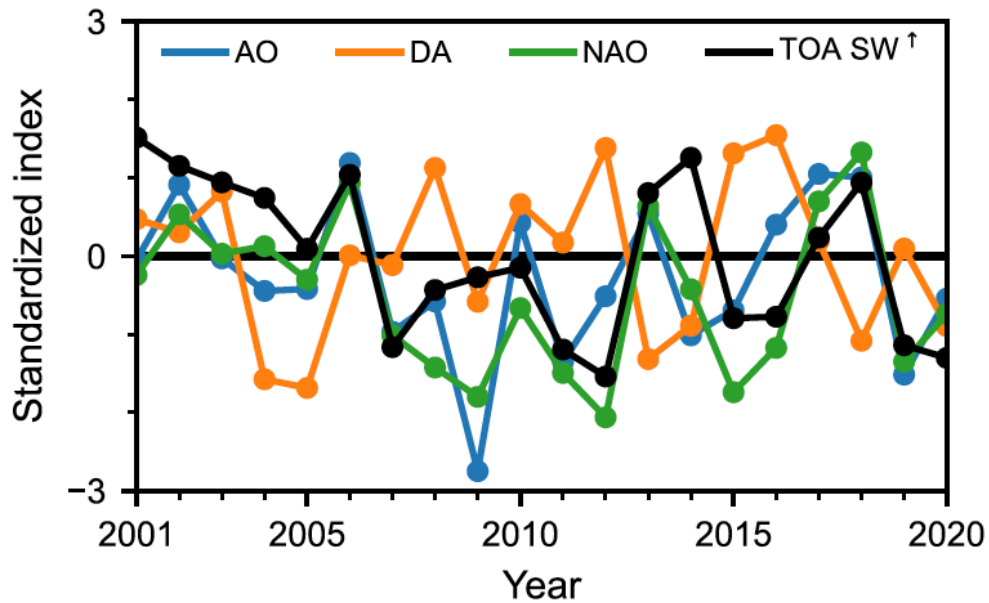
Discussion : Arctic Ocean



Sea ice age coverage of Arctic sea ice cover for the week of 12–18 March from 2001 to 2020.

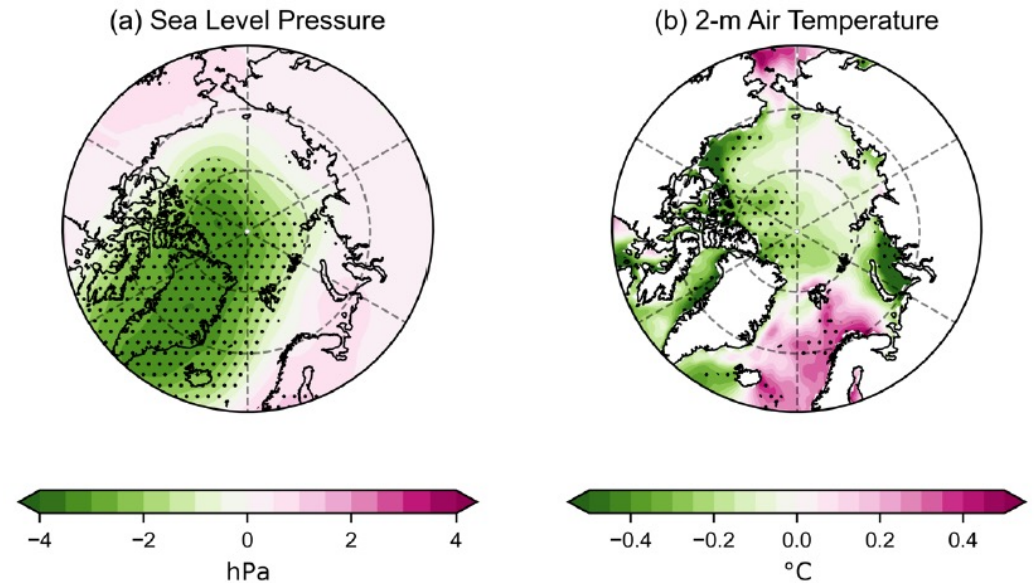
(Amma and Hayasaka 2023)

Discussion : North Atlantic Oscillation (NAO) and Arctic



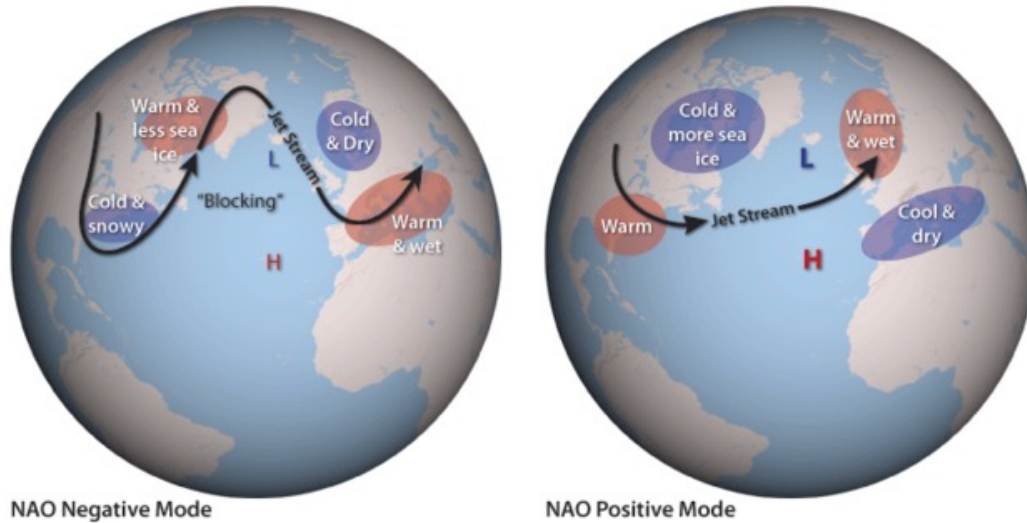
June and July mean standardized AO, DA, NAO indexes, and June and July mean standardized TOA SW anomaly over ocean.

AO: Arctic Oscillation, DA: Arctic Dipole Anomaly, NAO: North Atlantic Oscillation



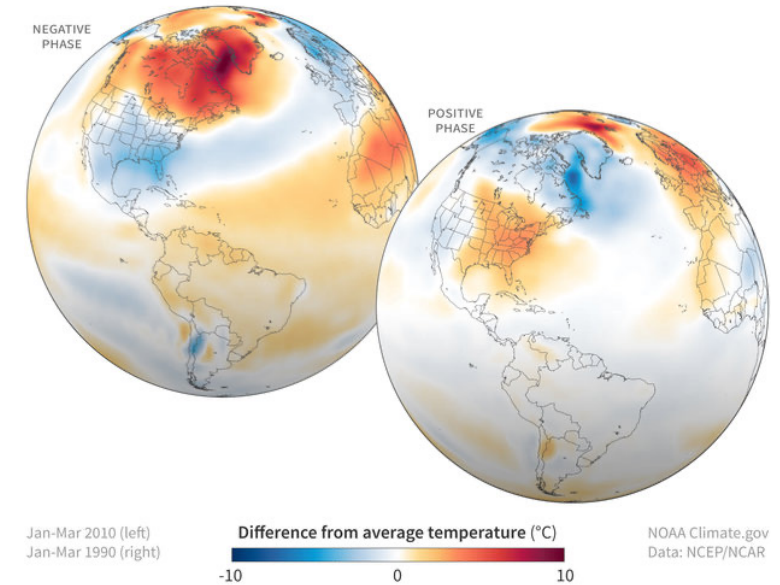
June and July mean (a) sea level pressure and (b) 2-m air temperature regressed onto the June and July mean NAO index. Dots indicate significance at the 95% level of Student's t-test

Discussion : North Atlantic Oscillation (NAO) and Arctic



On average, the surface pressure near Iceland is relatively low (L), while the pressure near the Azores Island is relatively high (H). During a negative phase (left), this pressure difference weakens. During a positive phase (right), the difference becomes even stronger than usual. The variation in pressure patterns influences the strength and location of the jet stream and the path of storms across the North Atlantic.

NAO TEMPERATURE PATTERNS



Late winter temperatures compared to the 1981-2010 average when the North Atlantic Oscillation (NAO) was strongly negative (top, Jan-March 2010) and when it was strongly positive (bottom, January-March 1990). Winters are often cooler than average across the mid-latitudes when the NAO is negative, and warmer than average when it is positive.

Summary

- Earth's radiation budget – The Earth is darkening for the past two decades.
- Variation in the SW radiation reflected at TOA is different among latitudes.
- Albedo change is consistent with variations in the Earthshine observation and SST.
- Earth's albedo is observed to be symmetry between NH and SH even for the darkening period.
- Difference of reflected SW radiation between NH and SH is related to the cloud variations.
- Aerosols do not contribute to the decreasing trend of albedo.
- El Neno, PDO, and Hiatus/Post-Hiatus climate modes may be related to the reflected SW radiation.
- Clouds, particularly low clouds and snow/ice are dominant factors for albedo variation.
- Sea ice is a major factor for the trend of SW radiation reflected at TOA in the Antarctic
- NAO and AO may be related to SW radiation reflected at TOA through sea ice in the Arctic.
- Albedo variation is consistent with variations in the atmosphere and SST, which supports the reliability of CERES observation.

References

- Amma, M. and T. Hayasaka, 2023: Interannual Variation in Top-of-Atmosphere Upward Shortwave Flux over the Arctic Related to Sea Ice, Snow Cover, and Land Cloud Cover in Spring and Summer. *J. Climate*, 36, doi: 10.1175/JCLI-D-22-0440.1. (in press)
- Blanco, J. E. et al., 2023: A Cloud-Controlling Factor Perspective on the Hemispheric Asymmetry of Extratropical Cloud Albedo. *J. Climate*, 36, 1793-1804, doi: 10.1175/JCLI-D-22-0410.1
- CERES Science Team Meeting, CERES webpage: <https://ceres.larc.nasa.gov/>
- Doelling, D. R. et al., 2013: Geostationary enhanced temporal interpolation for CERES flux products. *Journal of Atmospheric and Oceanic Technology*, 30, 1072–1090. <https://doi.org/10.1175/JTECH-D-12-00136.1>
- Goode, P. R. et al., 2021: Earth's albedo 1998–2017 as measured from earthshine. *Geophys. Res. Lett.*, 48, e2021GL094888. <https://doi.org/10.1029/2021GL094888>
- Gristey, J.J et al., 2021: Shortwave Radiance to Irradiance Conversion for Earth Radiation Budget Satellite Observations: A Review. *Remote Sens.* 13, 2640. <https://doi.org/10.3390/rs13132640>.
- IPCC, 2021: *Climate Change, 2021: The Physical Science Basis. Contribution of Working Group I to the Sixth Assessment Report of the Intergovernmental Panel on Climate Change.* Cambridge University Press, Cambridge, United Kingdom and New York, NY, USA, doi:10.1017/9781009157896.
- Jonsson, A. and F. A.-M. Bender, 2022: Persistence and Variability of Earth's Interhemispheric Albedo Symmetry in 19 Years of CERES EBAF Observations. *J. Climate*, 35, 249-268, doi: 10.1175/JCLI-D-20-0970.1.
- Lewis et al., 2010: Suomi Pragmatic Visionary. *Bull. Amer. Meteor. Soc.*, 91, 559-577.
- Liang, S., 2019: Remote sensing of earth's energy budget: synthesis and review, *International Journal of Digital Earth*, 12:7, 737-780, doi: 10.1080/17538947.2019.1597189.
- Loeb, N. G. et al., 2016: CERES top-of-atmosphere Earth radiation budget climate data record: Accounting for in-orbit changes in instrument calibration. *Remote Sensors*, 8, 182. <https://doi.org/10.3390/rs8030182>

References

- Loeb et al., 2018: Clouds and the Earth's Radiant Energy System (CERES) Energy Balanced and Filled (EBAF) Top-of-Atmosphere (TOA) Edition-4.0 Data Product. *J. Climate*, 31, 895-918, doi: 10.1175/JCLI-D-17-0208.1
- Loeb, N. G. et al., 2021: Satellite and ocean data reveal marked increase in Earth's heating rate. *Geophys. Res. Lett.*, 48, e2021GL093047. <https://doi.org/10.1029/2021GL093047>
- Loeb, N. G. et al., 2022: Evaluating twenty-year trends in Earth's energy flows from observations and reanalyses. *J. Geophys. Res.*, 127, e2022JD036686. <https://doi.org/10.1029/2022JD036686>.
- Montillet, J.-P. et al., 2022: Data fusion of total solar irradiance composite time series using 41 years of satellite measurements. *Journal of Geophysical Research: Atmospheres*, 127, e2021JD036146. <https://doi.org/10.1029/2021JD036146>.
- Qiu, J., P. et al., 2003: Earthshine and the Earth's albedo: 1. Earthshine observations and measurements of the lunar phase function for accurate measurements of the Earth's Bond albedo, *J. Geophys. Res.*, 108(D22), 4709, doi:10.1029/2003JD003610.
- Stephens, G. L. et al., 2015: The albedo of Earth, *Rev. Geophys.*, 53, 141–163, doi:10.1002/2014RG000449.
- Vonder Haar, T. H. and V. E. Suomi, 1969: Satellite observations of the earth's radiation budget. *Science*, 163, 667-669.
- Vonder Haar, T. H. and V. E. Suomi, 1971: Measurements of the Earth's radiation budget from satellite during a five-year period. Part I: Extended time and space means. *J. Atmos. Sci.*, 28, 305-314.
- Yu, Q. and Y. Huang, 2023: Distributions and trends of the aerosol direct radiative effect in the 21st century: Aerosol and environmental contributions. *J. Geophys. Res.*, 128, e2022JD037716. <https://doi.org/10.1029/2022JD037716>